CHALMERS
UNIVERSITY OF TECHNOLOGY

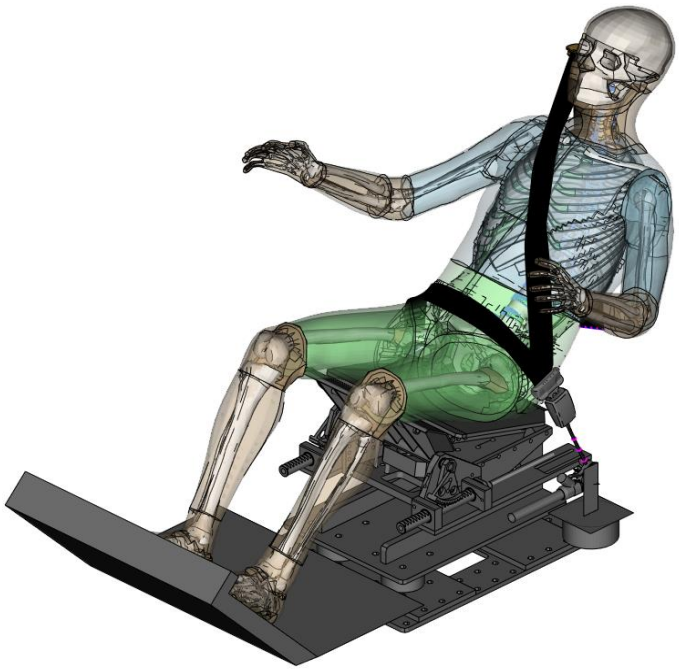

Validation of a Lumbar Spine Fracture Injury Criterion for Finite Element Human Body Model Simulations

Master's thesis in Applied Mechanics

Niklas Holländer
Seyed Ali Riazi

DEPARTMENT OF MECHANICS AND MARITIME SCIENCES
CHALMERS UNIVERSITY OF TECHNOLOGY

Gothenburg, Sweden 2023
www.chalmers.se

MASTER'S THESIS IN APPLIED MECHANICS

Validation of a Lumbar Spine Fracture Injury Criterion for Finite Element Human Body Model Simulations

Niklas Holländer, Seyed Ali Riazi

Department of Mechanics and Maritime Sciences
Division of Vehicle Safety
CHALMERS UNIVERSITY OF TECHNOLOGY
Göteborg, Sweden 2023

Validation of a Lumbar Spine Fracture Injury Criterion for Finite Element Human Body Model Simulations

Niklas Holländer, Seyed Ali Riazi

Master's Thesis
Department of Mechanics and Maritime Sciences
Division of Vehicle Safety
[Company Address]
Chalmers University of Technology
SE-412 96 Göteborg
Sweden
Telephone: + 46 (0)31-772 1000

Cover:
Human Body Model on the sled setup in a reclined position

Chalmers Reproservice / Department of Mechanics and Maritime Sciences
Göteborg, Sweden 2023-06-15

Validation of a Lumbar Spine Fracture Injury Criterion for Finite Element Human Body Model Simulations
Master's Thesis in Applied Mechanics
Niklas Holländer, Seyed Ali Riazi
Department of Mechanics and Maritime Sciences
Division of Vehicle Safety
Chalmers University of Technology

Abstract

Despite improvements in vehicle safety, leading to reduced moderate and severe injuries, in-depth studies on real-world vehicle crash data reveal that the risk of thoracic and lumbar spine fractures has not experienced a similar decline. This discrepancy may be attributed to the fact that thoracic and lumbar spinal injuries are not adequately assessed in vehicle safety regulations and consumer testing programs, potentially due to insufficient information or a limited understanding of the injury mechanism.

In this thesis, the aim was to validate a newly developed model of the human lumbar spine with an associated strain-based fracture injury risk function (IRF). To reach this aim, the new lumbar spine model was used in reconstructions of tests on isolated lumbar spines, the lumbar spine model was integrated in the SAFER Human Body Model (HBM) and the updated model was used in reconstructions of sled tests with Post Mortem Human Subjects (PMHSs) in reclined positions and of a real accident. The risks of lumbar spine injury fractures were estimated using the proposed strain-based injury criterion and compared with the injury scores from the original tests and in the accident and with other those from recently proposed force based lumbar spine fracture injury risk functions. In addition to the HBM simulations, an FE model of the Test device for Human Occupant Restraint (THOR) used in reconstructions of the sled tests to assess the comparability of the proposed IRF and the measurements obtained from the THOR FE model.

For the isolated lumbar spine validations, the results indicated that the first lumbar vertebra (L1) had the highest risk of fracture, which was consistent with the experimental findings, and in the non-injurious case, the predicted risks were low at all vertebral levels. In the whole-body validation, the reconstruction indicated a high risk of L1 fracture. This was consistent with the findings from the laboratory tests, in which 3 out of 5 PMHSs experiencing fractures at L1 during the experiments. In the accident reconstruction, for which the occupant experienced a fracture at L5, there was an estimated fracture risk in the reconstruction of with the highest value of approximately 70% at L5. However, the force-based injury criteria showed low fracture risk in both the reconstructions of the sled tests and the accident, indicating a lower ability to predict risk of fractures. The new lumbar spine model and strain-based IRF appear to appropriately predict the risk of lumbar spine fractures when used isolated and when used as an integrated unit in a complete HBM. The result of the THOR simulation revealed a significant dependence on variations in H-point position on the THOR-sled FE model.

Keywords: Human Body Model, Finite Element, Injury Criteria, THOR, Lumbar Spine

Contents

Preface

This master thesis project was carried out at the Volvo Cars Safety Centre in Torslanda, Gothenburg, Sweden during the spring semester of 2023.

Acknowledgements

We would like to express our heartfelt appreciation to all those who have provided invaluable assistance and support throughout the completion of our master's thesis and our time at Chalmers University of Technology. Over the years, we have been fortunate to encounter numerous individuals who have greatly contributed to our personal growth and accomplishments.

First and foremost, we extend our deepest gratitude to **Volvo Car Corporation** for granting us the opportunity to undertake this master's thesis. Especially, **Jonas Östh**, our supervisor, for supervision in the art of writing papers, preparing presentations and for generous advice and encouragement throughout our thesis.

We would also like to acknowledge **Johan Davidsson**, whose previous work laid the foundation for our thesis, as well being the examiner for our thesis.

Our appreciation extends to **Anders Bernhardsson** from **DYNAmore Nordic** for holding the LS-DYNA course, which provided us with essential knowledge. We are also thankful for the continued support we received for LS-DYNA even after the course concluded.

We would also like to thank **Jonas Bärgman** for holding the Academic Writing course. Providing us with further knowledge within the art of writing.

We express our gratitude to **Peter Appelgren** for his assistance with ANSA and META support.

Our heartfelt thanks go to the entire **Injury Prevention Principles and Guidelines Team** at Volvo Cars Safety Centre in Torslanda.

Furthermore, we would like to acknowledge the master’s thesis students at Volvo Cars Safety Centre; **Kristoffer Karlsson, Khashayar Asadi, Ellen Ryckenberg** and **Emma Djerf**. For their help and moral support, and for a very pleasant working atmosphere.

Finally, we are grateful to our families and friends for support and patience throughout our thesis.

Göteborg 2023-06-15

Niklas Holländer, Seyed Ali Riazi

Notations

ATD	Anthropomorphic Test Device
CoG	Centre of Gravity
EDR	Event Data Recorder
FE	Finite Element
FSU	Functional Spine Unit
HBM	Human Body Model
IARV	Injury Assessment Reference Value
IC	Injury Criterion
IRF	Injury Risk Function
NHTSA	National Highway Traffic Safety Administration
PDB	Partnership for Dummy Technology and Biomechanics
PLL	Posterior Longitudinal Ligament
PMHS	Post-Mortem Human Subject
PMMA	Polymethyl Methacrylate
THOR	Test device for Human Occupant Restraint
WHO	World Health Organization
F	Compressive axial force
F_r	Resultant compressive force
F_z	Compressive force in z-direction
M_r	Resultant Bending Moment
Δv	Velocity change
μCT	X-ray microtomography

1 Introduction

Traffic fatalities account for 1.35 million people annually, according to the World Health Organization (WHO 2018). That is many lives lost to a seemingly preventable cause, making traffic accidents the 8th leading cause of death for individuals of all ages. The WHO notes that vehicle occupants account for a significant portion of road fatalities, with 29% of the total casualties. Vehicle safety has improved over the years, leading to a considerable reduction in moderate and severe injuries, according to National Highway Traffic Safety Administration (NHTSA 2019). However, detailed studies of real-world crash data on the risk of spine fracture (Pintar *et al.* 2012; Jakobsson et al. 2016), show that the incidence for thoracic and lumbar spine fractures has not been reduced in a similar way, but might even have increased for newer vehicle model years (Pintar *et al*. 2012). This difference could be caused by that thoracic and lumbar spinal injuries are not assessed in vehicle regulations and consumer testing, perhaps due to a lack of information or poorly understood injury mechanism (Pintar *et al.* 2012).

An early investigation on the response of the vertebral column was conducted by Begeman *et al.* (1973). They employed Anthropomorphic Test Devices (ATDs) in planar motion to determine an axial load along the spine and its load on the seat pan. However, they noted that the lack of spinal curvature in ATDs restrict their usefulness for assessment of spinal loads. Zheng *et al.* (2017) conducted a more recent study to investigate the capacity of a detailed Finite Element (FE) model of the human lumbar spine. They utilized lumbar compression fracture experiments on Post-Mortem Human Subjects (PMHS) that had been conducted by others over several years to validate their developed human lumbar spine FE model. One of the experimental studies were carried out by Duma *et al.* (2006) and investigated the biomechanical responses of the lumbar spine to dynamic compression. Duma *et al.* (2006) showed that lumbar fracture can occur at a combination of axial load and bending moments. Furthermore, they highlighted that most studies only report axial load as a lumbar fracture tolerance, despite the occurrence of bending moments. More recent experiments on PMHS conducted by Stemper *et al.* (2011; 2018) utilized a drop-tower method to capture pelvis acceleration as an indirect measure of spinal loads. They showed that peak axial force and peak acceleration were strong predictors of injury. Based on these findings, they used both peak compressive F_z force and vertical pelvis acceleration as Injury Criteria (IC) for lumbar spine fracture and created Injury Risk Functions (IRFs) for the probability of injury for the average male.

According to studies conducted recently by Östling *et al.* (2019), the use of highly automated or "self-driving" vehicles could enable occupants to assume more reclined postures that differ from the traditional upright, forward-facing position. Furthermore, that the injury mechanisms of the lumbar spine depend significantly on the flexed spine curvature of the vehicle occupant was shown by Oritz-Paparoni *et al*. (2021) through testing of Post Mortem Human Subject (PMHS) spines to fracture in varying spinal postures. Reclined seating postures could alter occupant's kinematics and challenge current restraint designs, increasing the need for improved understanding of lumbar spine injury mechanism according to Richardson *et al*. (2020).

The estimation of lumbar spine injury risks currently relies on cross sectional forces and moments, utilizing IRFs derived from biomechanical testing (Yoganandan *et al*. 2020). Examples are the IC and IRFs proposed by Stemper *et al.* (2018). These IRFs

can work sufficiently when a mid-sized Human Body Model (HBM) are used, but it is insufficient for morphed (size, shape and proportion scaled) HBMs (Larsson *et al.* 2022), as most IRFs normally do not include size dependent covariates. An appealing approach to assess lumbar spine injury risks using HBMs is to employ a tissue based IRF, using metrics such as stress or strain, that inherently scales with the dimensions of the spine. Hence, in a recent study by Iraeus *et al.* (2023) developed a new detailed FE lumbar spine model at SAFER, Vehicle and Traffic Safety Centre at Chalmers University of Technology, Gothenburg, Sweden. This model was targeted for inclusion in HBMs and use in design of vehicle restraints. The authors validated the model kinetics and kinematics using published biomechanical data. They also developed a strain-based IC in the inferior-superior Z-direction in the trabecular bone and its associated IRF for compression fractures in the vertebrae, using lumbar spine Functional Spine Unit (FSU) tests, in which FSUs consisting of two to three lumbar spine vertebrae were loaded to fracture.

1.1 Aim

The first aim of this study is to evaluate the predictive capacity of a newly proposed strain-based IC and its associated Injury Risk Function for lumbar vertebra fracture using a Finite Element Human Body Model, in comparison to Post-Mortem Human Subjects experiments, and benchmark it with respect to other newly proposed lumbar vertebra fracture IC and IRFs. A secondary aim is to further compare the FE HBM and IRF predictions with lumbar spine measurements that can be made using an FE model of the most advanced frontal impact dummy, the THOR.

2 Background

Human Body Models serve as computational representations of the living human body and are used to study its biomechanical response, particularly in injurious impact scenarios. To bridge the gap between HBMs simulations and real-world injury probability, injury risk functions computing the risk of sustaining an injury are used with the outputs from the HBMs.

2.1 Impact Biomechanics

Impact biomechanics is the study of the mechanical response of the human body to an external impact, such as a fall or collision. This field of research is crucial in understanding and preventing injuries related to impact, particularly in high-risk activities such as sports, military operations, and automotive (Schmitt *et al.* 2019). The biomechanical response of the body to an impact can be complex, and depends on various factors including the impact velocity, the location and direction of the impact, and the age and physical condition of the individual. The primary goal of impact biomechanics is to quantify and understand the biomechanical response of the body to these factors, to develop effective injury prevention strategies (Schmitt *et al.* 2019).

To study the biomechanical response of the human body, researchers commonly use five different experiment models: human volunteers, human cadavers, animals, human surrogates (ATDs), and mathematical models.

Human volunteer experiments are limited to low severity ranges to avoid causing injuries. Mechanical loads are applied up to the pain threshold. Volunteer tests offer advantages like anatomical and physiological accuracy, the ability to study muscle tone and bracing effects. However, the cohorts used in volunteer tests are often not representative of the population at risk, lacking diversity in terms of sex, age, and other factors (Schmitt *et al.* 2019).

Human cadavers, usually denoted PMHS in literature are the second type of experiment to determine the human biomechanical response. PMHS have a great anatomical similarity to the living human. However, age-related degeneration, lack of muscle tone and variations in preparation techniques can influence the test results (Schmitt *et al.* 2019).

Animal experiments are used in impact biomechanics, but its relevance is limited. However, anesthetized animals provide a way for studying physiological responses to severe mechanical loads. Animal experiments also enable a comparison between living and deceased tissues, offering valuable insights for the accurate interpretation of cadaver tests (Schmitt *et al.* 2019).

An ATD is mechanical model of the human body used as a human surrogate in crash testing. ATDs are constructed to measure mechanical loading parameters during impacts that would pose a risk of injury to a living human. These dummies are made from steel or aluminum for the skeleton, polymers for the joints surface and skin, and foam for flesh simulation. They are equipped with multiple accelerometers and load cells to capture data on acceleration, force, or deformation. Various types of ATDs exist to this date, with each one designed to capture a specific type of impact (Schmitt *et al.* 2019). For instance, like the most recently developed frontal impact ATD, THOR.

Finally, due to rapid improvement in computational power, software analysis (i.e., FE codes), and data for human body modeling, computer simulations have become a crucial tool in impact biomechanics, providing valuable insights that were previously inaccessible. They are widely used in safety engineering fields, including vehicle crashworthiness design and accident reconstruction, contributing to safety enhancements. Advanced HBM allows for analyzing scenarios that cannot be directly tested. For instance, live humans in injurious impact scenarios (Schmitt *et al.* 2019).

2.2 Explicit Finite Element Method

The explicit method is a widely used numerical method for solving nonlinear problems using FE analysis in softwares such as LS-DYNA (ANSYS/LST, Livermore, CA, USA), which was used in this thesis. It is particularly useful for simulating problems with short transient times and moderate deformation responses, such as impact and explosion simulations, dynamic response of structures, and crashworthiness analysis.

In the explicit method, the equations of motion are discretized in time and solved explicitly, step by step. This means that the solution at each time step is computed based on the solution at the previous time step, without having to solve a system of equations (i.e implicit). The method is called explicit because the time-dependent terms in the equations of motion are explicitly accounted for in the solution procedure (Belytschko *et al*. 2014).

To ensure the stability and accuracy of the explicit method, the time step size must be carefully chosen. The time step size should be small enough to capture the high-frequency response of the material, considering the material stiffness and damping, but large enough to ensure the computational efficiency of the method. LS-DYNA is using central differencing, which is a conditionally stable time integration method in explicit dynamics, but its accuracy and efficiency depends on the critical time step size (Belytschko *et al*. 2014).

2.3 Finite Element Human Body Models

Finite element human body models are computational representations of the human body that utilize the finite element method. These models involve dividing the human body into discrete finite elements, such as tetrahedrons or hexahedrons, representing various anatomical structures and tissues. FE HBMs are widely used in biomechanics, crashworthiness analysis, and injury prediction. By applying boundary conditions and loading scenarios, FE HBMs can simulate and predict how the human body deforms, strains, and experiences stress during different crashes or events. They play a crucial role in studying impact responses, assessing injury risks, and optimizing safety measures (Schmitt *et al.* 2019).

Finite element human body models require careful consideration of factors such as size, material properties, and interaction between body parts. Model validation against experimental data, such as PMHS tests or injury databases, is crucial to ensure their accuracy and reliability (Schmitt *et al.* 2019).

The SAFER FE HBM v10, Figure 1, used in this thesis, represents a 50^{th} percentile male (175 cm, 77 kg) occupant, and was originally based on THUMS v3. However, the model has undergone significant updates and replacements, particularly in its latest version, v10. Notable updates include the replacement of the head with the KTH Royal Institute of Technology (KTH) head model. Additionally, the rib cage has been replaced

with a statistically derived 50th percentile male shape, and the cervical and lumbar spine have been updated. To simulate human postural control during a pre-crash phase, the model incorporates an active muscle package that utilizes feedback control mechanisms (Östh *et al.* 2021).

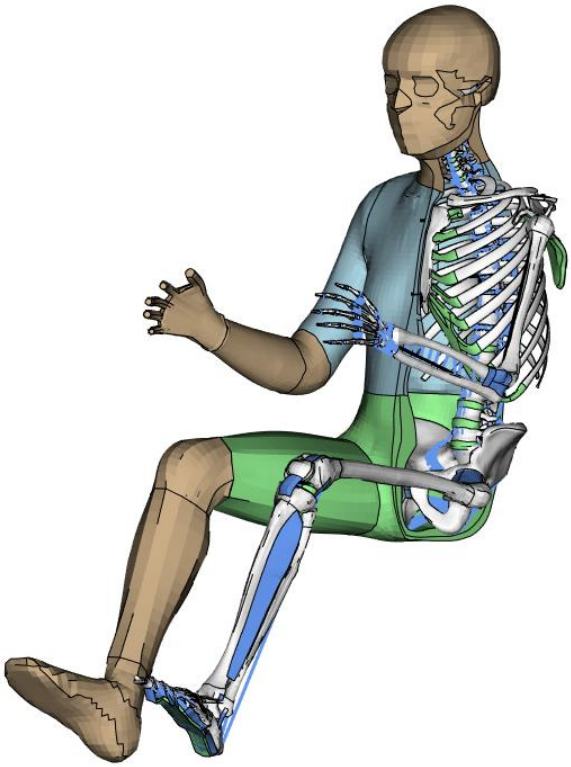

Figure 1. The SAFER HBM v10.0 in an upright seated occupant position.

2.3.1 Lumbar Spine FE Model

The new lumbar spine FE model that will be used in this study was developed by Iraeus *et al.* (2023), Figure 2.

The lumbar spine finite element (FE) model was designed based on the geometry of an average-sized female. Reduced-order hexahedral elements were employed to model the trabecular bone, while fully integrated elements were utilized for the cortical bone and endplates. In addition, an elastic orthotropic material model was applied to represent the trabecular bone to capture compression fractures. In LS-DYNA, the material model featured Young's modulus of 49.2 MPa in the main direction (inferior-superior), with all other orthotropic constants perpendicular and scaled from the main direction. The lumbar spine FE model had pre-defined cross sections in each lumbar spinal level, where forces and moments could be measured in the model.

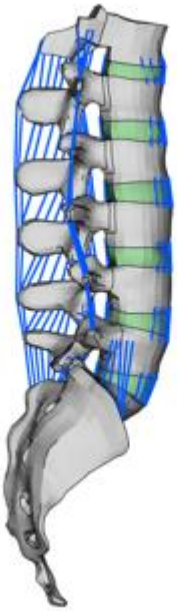

Figure 2. The new FE-model of the lumbar spine (L1-L5) developed by Iraeus et al. (2023), scaled to average male size to fit the SAFER HBM.

The model employed a hexagonal block design with mesh quality criteria based on Pipkorn et al. (2021), which targets a minimum aspect ratio limit of less than 3 for 95% of the elements and a maximum limit of 10 for 100% of the elements, applicable to both shells and solids. Additionally, the Jacobian was set to target a maximum limit of greater than 0.7 for 95% of the elements and 0.3 for 100% of the elements. As a result of the mesh quality check, all elements fell within the designated ranges of the mesh quality criteria.

2.4 Injury Criteria and Injury Risk Function

Injury criteria are crucial tools for assessing the severity of accidental loading and the associated risk of injury in impact biomechanics. An injury criterion establishes a relationship between physical parameters (such as acceleration or force) and the probability of injury to specific body regions (i.e., whiplash or lumbar vertebra fracture). To develop injury criteria, a combination of experimental studies on PMHS and empirical evidence is used. This process involves a detailed and step-by-step extrapolation procedure due to the ethical constraints that prohibit conducting traumatic experiments on living humans (Schmitt *et al.* 2019), while an injury criterion is intended to describe the property of a living human.

Each injury criterion is associated with a specific risk function (the IRF) that determines the likelihood of sustaining an injury at a particular severity level. The IRF incorporates the computed values of the injury criteria into its formula to calculate the risk. The injury criteria are based on different distributions, either Weibull or log-normal, depending on the specific function they were designed for. The risk functions have distinct parameter values for each individual criterion.

2.5 Lumbar Spine Injury Criteria

Below presents the injury criteria for lumbar vertebra fracture and their associated IRFs that were assessed in this thesis.

2.5.1 Chalmers Strain-Based Injury Criteria

Klein and Davidsson (2023) developed an endplate fracture IRF with the new lumbar spine FE model utilizing the maximum inferior-superior compressive Z-strain, (Figure 3), in the trabecular bone. The IRF was constructed using data from tests that were loaded with compression or compression combined with flexion and or compression followed by flexion. Resulted in a total of 119 specimens with most male specimens. The reconstruction of the tests included FE simulations using FSUs of a generic lumbar spine FE model, with two or three adjacent spine vertebrae, to finalize the IRF.

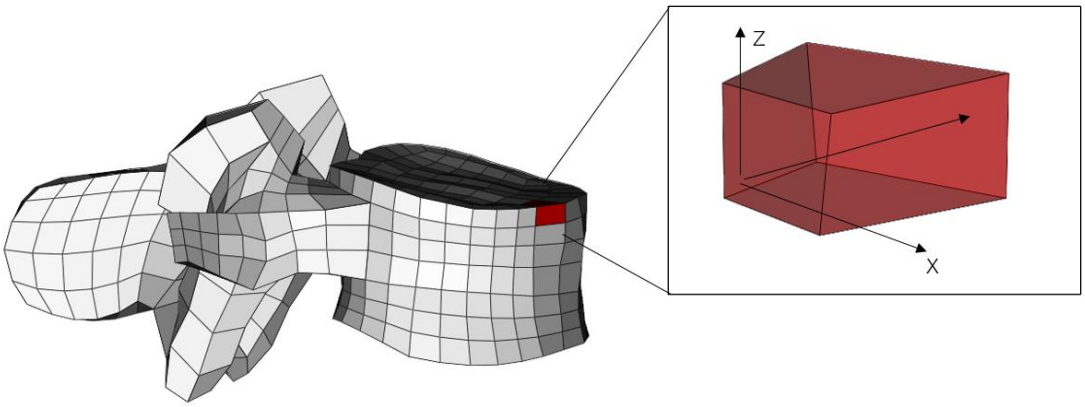

Figure 3. Illustration of the material coordinate system in the trabecular bone.

The author's statistical analysis revealed that the best model included age and sex covariates in the IRF. The age covariate refers to the subject's age in years, while the sex covariate is represented by the values 0 for females and 1 for males. Equation (1) represents the IRF and the risk according to the log-normal distribution., with coefficients given in Table 1. Curves for a model representative a 50-year-old female and a 50-year-old male are shown in Figure 4.

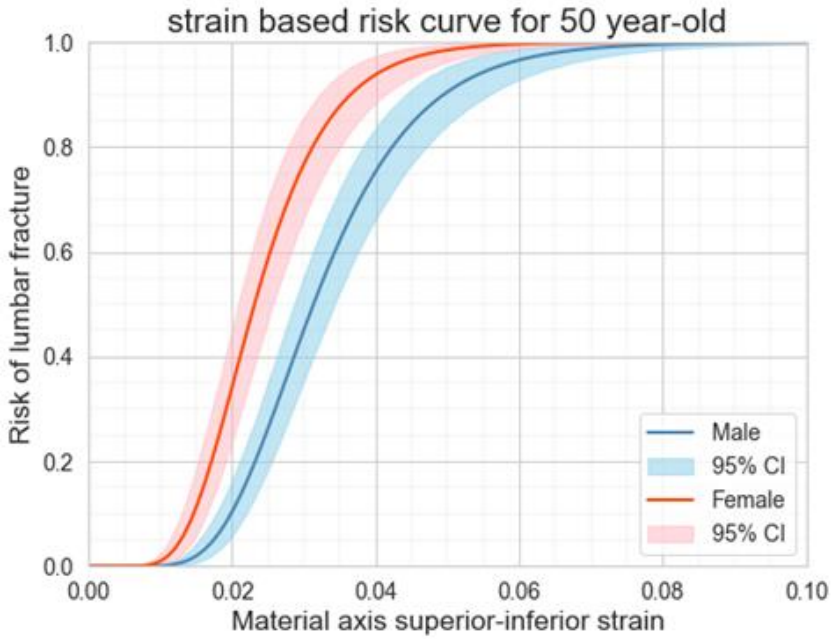

Figure 4. Injury risk curves for a 50-year-old female and a 50-year-old male including respective 95% Confidential Interval (CI) using the new lumbar spine FE model (Klein and Davidsson 2023).

.

$$\text{Risk} = \frac{1}{2} + \frac{1}{2}\text{erf}\left(\frac{\ln(\text{strain}) - (\beta_1 + \text{age} * \text{coef}_{\text{age}} + \text{sex} * \text{coef}_{\text{sex}})}{\sqrt{2 * (\exp(\beta_2))^2}}\right) \quad (1)$$

Table 1. The parameters for the injury risk function proposed by Klein and Davidsson. (2023).

β_1	β_2	coef_{age}	coef_{sex}
3.1178	-1.0314	-0.0118	0.3045

2.5.2 Tushak Force and Moment-Based Injury Criterion

Tushak *et al.* (2022) used a beam theory based IRF input metric, in which the lumbar spine was modelled as a beam subjected to a combination of stresses from compressive axial force (*F*) and bending moment (*M*). The authors developed a lumbar vertebra fracture criterion, defined as the variable L_{fx} (Equation 2).

$$L_{fx(t)} = (1 - \alpha)\frac{F(t)}{CSA} + \alpha\frac{M(t)}{CSA^{3/2}} \quad (2)$$

The IC equation is a linear combination of stress-like terms: normalized axial compression and normalized flexion moment. *CSA* is the area of the superior endplate, α is a relative contribution factor, to produce the IRF with best predictive fit to the data and was optimized resulting with a value of 0.11. The IRF was fit using data from 40 3-vertebrae lumbar spine FSUs with an average donor age of 49 years. Equation (3)

represents the IRF and the risk according to the Weibull distribution. Where L_{fx} in units of MPa, the coefficients of the intercept, scale, and age covariate.

$$P\left(fracture\middle|L_{fx}, Age\right) = 1 - e^{-\left(\frac{L_{fx}}{e^{1.89043-0.00886*Age}}\right)^{\frac{1}{0.201}}} \quad (3)$$

2.5.3 Ortiz-Paparoni Force and Moment-Based Injury Criterion

Ortiz-Paparoni *et al.* (2021) developed an IRF (L_{ic}) that were derived by combining the T12-L1 resultant compressive force (F_r) and the decorrelated bending moment (M_y) into a combined metric (κ), Equation (5). The IRF was fit using data from 75 thoracolumbar male specimens with an average donor of 66 years. The location of the decorrelated bending moment and scale parameters of the log-normal cumulative density function, which yielded values of -0.0578 and 0.3214, respectively, Equation (4).

$$\kappa = \frac{F_r}{5824} + \frac{M_y}{1155} \quad (4)$$

$$L_{ic}(\kappa; -0.0578, 0.3214) = \frac{1}{2} + \frac{1}{2}\text{erf}\left(\frac{\ln(\kappa) - 0.0578}{0.3214 * \sqrt{2}}\right) \quad (5)$$

2.5.4 Stemper Force-Based Injury Criterion

Stemper *et al.* (2018) developed Injury Risk Curves (IRCs) for the average male with a Weibull distribution derived by the peak compressive F_z force and pelvis acceleration as injury criteria for lumbar spine fracture, (Figure 5). The developed IRCs was fitted using 23 intact human lumbar spine from T12 to L5 with an average donor age of 49 years.

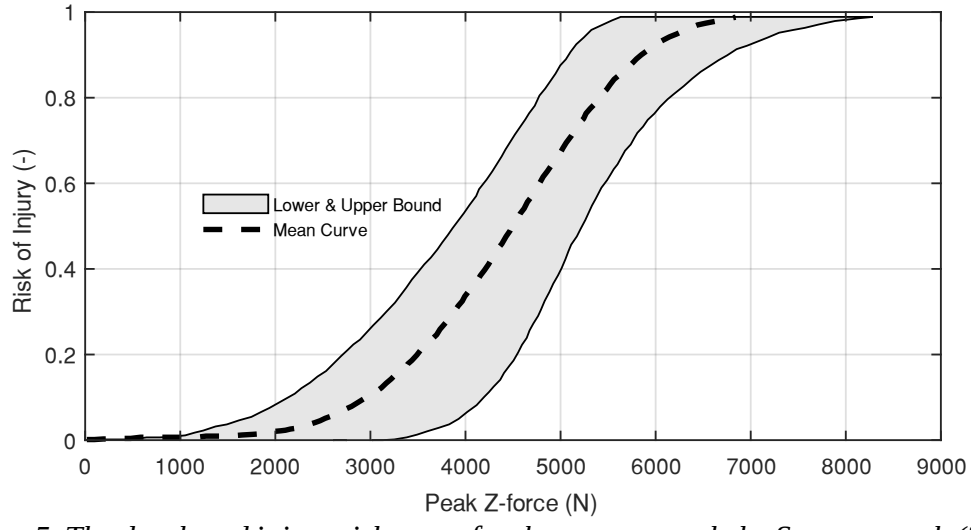

Figure 5. The developed injury risk curve for the average male by Stemper et al. (2018). The plot shows the mean curve and 95% confidence intervals.

2.6 Lumbar Injury Reference Assessment Value

In addition, to the lumbar spine injury criterion, an engineering Injury Assessment Reference Value (IARV) was calculated, called L_{Index}. The IARV contains a compressive axial force in z-direction (F_z) and a resultant bending moment (M_r). If L_{Index} value is below 1 then no occurrence of lumbar vertebra fracture. The critical parameters in Equation (6). that were used was $F_{z,crit} = 4.5$ kN and $M_{r,crit} = 180$ Nm, based on the mean lumbar failure force from Stemper *et al.* (2018) and the lumbar flexion failure moment from Belwadi and Yang (2008).

$$L_{index} = \frac{F_z}{F_{z,crit}} + \frac{M_r}{M_{r,crit}} \leq 1 \quad (6)$$

3 Method

The work conducted in this study was based on the FE-model of SAFER HBM and THOR. The work was divided into three sections: validation of the isolated lumbar spine, validation of the whole HBM and THOR FE-model in sled test laboratory setting, and finally, FE-model in an accident reconstruction application vehicle setting.

3.1 FE Human Body Models and ATD FE-Model

The HBM used in this study was based on SAFER HBM v10. In this version of the HBM which was used here, the new lumbar spine of the model was updated compared to the SAFER HBM v10. From here on, the HBM with the updated lumbar spine will be referred to as SAFER HBM v10X.

The isolated lumbar spine validation involved using both the newly updated lumbar spine and the lumbar spine from SAFER HBM v10. Furthermore, the validation of the whole-body sled test laboratory setting, and assessment of the accident reconstruction used and compared both SAFER HBM v10 and SAFER HBM v10X.

The Dummy FE-model used here in the sled setup was the THOR-50M Standard Build Level B (SBL-B) ATD USNCAP version 1.7 (Humanetics, 2020).

3.2 Pre-processing Tools

The simulations configurations were pre-processed using ANSA version 23.1.0 (Beta CAE Systems, Luzern, Switzerland). The FE simulations of chapters 3.3.1 and 3.4 were run with the explicit solver LS-DYNA MPP R9.3.1 Single Precision (LSTC, Livermore, CA), and for chapters 3.3.2 and 3.7 LS-DYNA R12.1 was used. For positioning and seatbelt routing of the HBM and THOR were created in PRIMER version 19 (OASYS, Solihull, UK).

3.3 Isolated Lumbar Spine Validation

The isolated lumbar spine validation was separated into simulation of two types of experiments: Injurious and non-injurious PMHS experiments. The injurious PMHS experiment was conducted by Stemper *et al.* (2018) and included 23 specimens for which a majority showed no major degeneration changes in the pre-test grading. The available data presented 17 specimens where the age range was between 18 – 63 years, including nine females and eight males. The most common injury affected the L1 vertebra level (13/26).

The non-injurious PMHS experiment conducted by Ortiz-Paparoni *et al.* (2020) included three PMHS lumbar spine that were dissected from male whole-body donors. The demographic data available for all specimens were age (74 ± 6.9 years) and weight (74.8 ± 25.6 kg). Two of the three specimens' heights were available, 177.8 and 167.6 cm. The authors reported no injury to the lumbar spine after testing. The objective of the isolated lumbar spine validation was to assess the ability of the IRF proposed by Klein and Davidsson (2023) to separate between injured and non-injured on an isolated lumbar spine level, and not only on functional spine unit (FSU) level for which the IC and IRF was developed.

3.3.1 Injurious Experiment Validation

Stemper *et al.* (2018) aimed to replicating the loads experienced by the lumbar spine under high vertical acceleration, for instance in emergency ejection of pilots from aircraft. The test setup consisted of a monorail holding two horizontal platforms. The platforms could only move vertically downwards and upwards. A pulse-shaping foam was located at the bottom of the setup at which the impact took place. Polymethylmethacrylate (PMMA) was utilized to secure the cranial and caudal ends of the lumbar spine to the loading device. Attachment of the specimen to the lower platform was achieved through a six-axis load cell. Measures were taken to prevent slippage between the upper platform and the superior PMMA fixation. Accelerometers were placed on the upper and lower platform to detect and record the acceleration of the impact. Stemper *et al.* (2011) recorded a time history of the vertical acceleration of the lower platform of one of the experiments with a peak acceleration of 13 g (Figure 6).

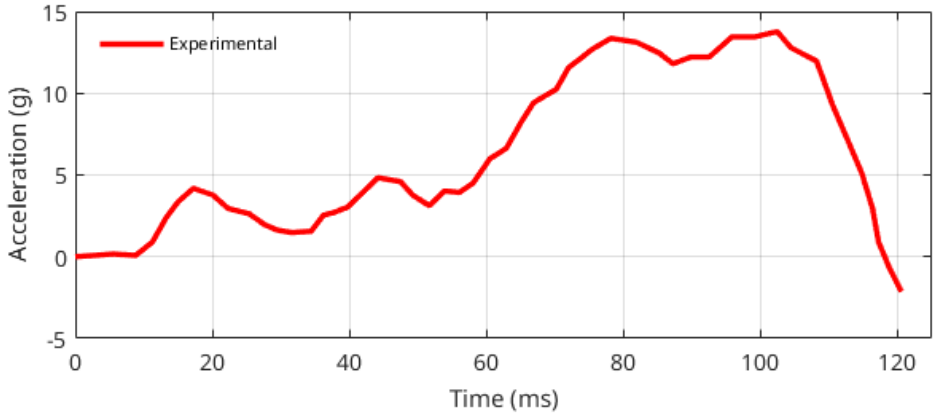

Figure 6. Vertical acceleration versus time of the lower platform during one of the experiments measured at the lower platform by Stemper et al. (2011).

Stemper *et al.* (2011) reported that the natural lordotic curvature for each specimen was not changed during the positioning of the lumbar spine, and that the L2-L3 disc was kept nearly horizontal with respect to the global horizontal axis. The point of contact range between the cranial fixation and the upper platform was located at around 3.0-3.5 cm anterior to the L2-L3 Posterior Longitudinal Ligament (PLL).

3.3.1.1 Simulation Setup

Both the lumbar spine from SAFER HBM v10 and the updated lumbar spine was used to reconstruct the experiment explained above. Here the ligamentous spine was used, which includes both the vertebral body and the intervertebral disc components of the lumbar spine, and the ligaments. The FE model of the lumbar spine was positioned between the upper and lower platform which were defined as rigid bodies (Figure 7). The lower PMMA-fixation was connected to Rigid Body 2 and is free to rotate in any direction. A deformable body was then added between Rigid Body 2 and Rigid Body 3 to replicate the load cell in the experiment test. The load cell forces were extracted of a cross-section through the deformable body. To represent the torso mass for 50th percentile male (175 cm, 77 kg) in the experiment, a 32 kg mass was added to the upper platform.

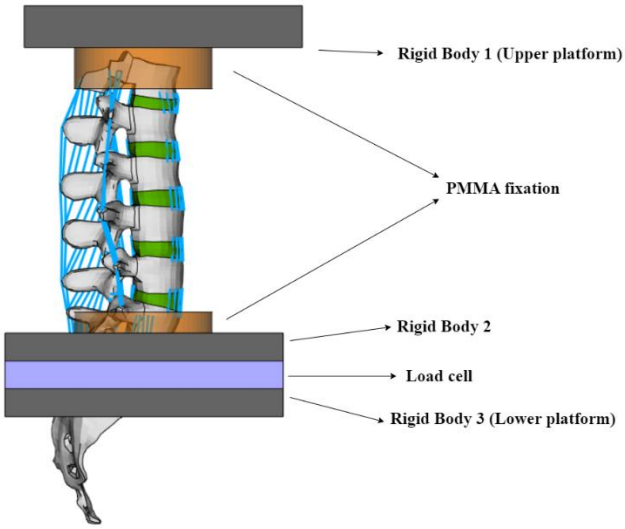

Figure 7. The simulation setup based on Stemper et al. (2018) experiment.

At the center of gravity (CoG) of Rigid Body 1, a revolute joint was used to connect the upper PMMA fixation and Rigid Body 1. The recorded acceleration of the lower platform from the experiment setup, Figure 6, was applied as a boundary condition to the lower platform. Rigid Body 1 (Upper platform) and Rigid Body 3 (Lower platform) can only move in vertical direction and restricted to move and rotate in other directions.

3.3.1.2 Parameter Study

To investigate the sensitivity of the simulation setup, a minor parameter study was performed by shifting the CoG of Rigid Body 1, where the revolute joint was located, anteriorly along the sagittal axis from L2-L3 PLL axis (Figure 8). The variation was based on the description of the experimental setup. The study included 5 different positions of Rigid Body CoG. Table 2 displays the distance of the Rigid Body 1 from L2-L3 PLL with the corresponding simulation labelled from 1-5. Simulation 1 is where the Rigid Body 1 CoG closet to the L2-L3 PLL axis, while Simulation 5 is the furthest position. Simulation 3 were aligned within the point of contact range between the cranial fixation and upper platform that Stemper *et al.* (2018) reported.

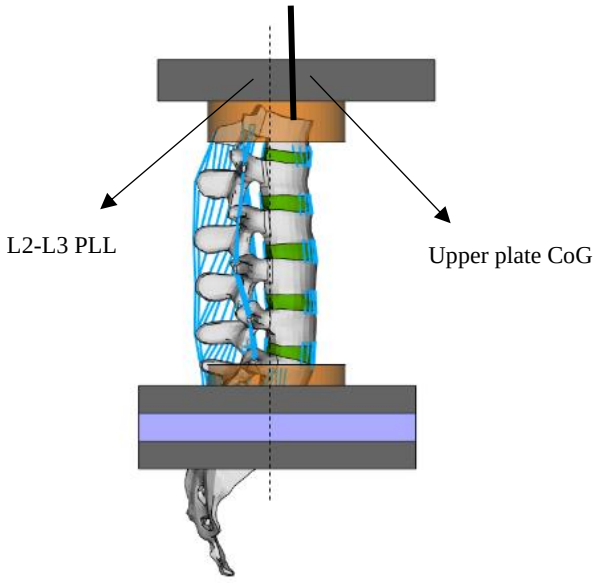

Figure 8: Location of the upper plate CoG relative to L2-L3 posterior longitudinal ligament showed in dashed line.

Table 2. Parametric study containing the position of Rigid Body 1 center of gravity (CoG) from L2-L3 PLL.

Simulation	1	2	3	4	5
Rigid Body 1 CoG (cm)	2.3	2.8	3.3	3.8	4.1

3.3.2 Non-injurious Experiment Validation

3.3.2.1 Experiment Setup

Ortiz-Paparoni *et al.* (2020) aimed to assess the structural response of three post-mortem human subject lumbar spines using μCT images and perform dynamic compression testing on the thoracolumbar spine. In the test setup, T12 and S1 in the lumbar spine were fixed to the casting materials using screws and k-wires, wrapped with PMMA. The position of the lumbar spine was aligned with the nominal posture by seated soldier study by Reed *et al.* (2013). Prior to testing, 1 Hz oscillatory pulse at 1% strain for five minutes was applied to the specimens for preconditioning. Then the lumbar spines were subjected to three non-injurious dynamic compression conditions at rates 200, 400, and 600 N/ms. Ortiz-Paparoni *et al.* (2020) concluded that the proposed loading rate corresponds to the lower end of the under-body blast loading regime. The applied load and moment responses were recorded by a 6-axis load cell.

3.3.2.2 Simulation Setup

The simulation setup comprised of the lumbar spine, which was placed between two potting cups with T12 and S1 encased in PMMA. To attain the seated soldier's posture, with the mid vertebral body of T12 at 2 degrees in extension and the S1 superior endplate at 10 degrees in extension, a pre-simulation was made to position the spine (Figure 9). The positioning procedure involved a rigid constraint between the upper-cup and T12 upper endplate, followed by manipulation of the upper-cup through movement and rotation (Figure 10). The upward dynamic loads were applied to the lower potting cup.

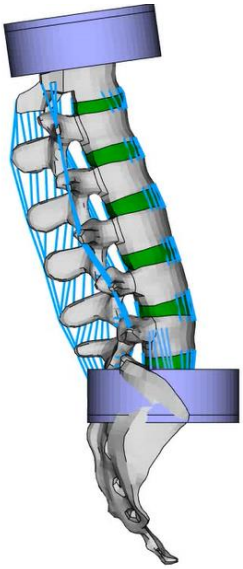

Figure 9. Initial posture of the lumbar spine.

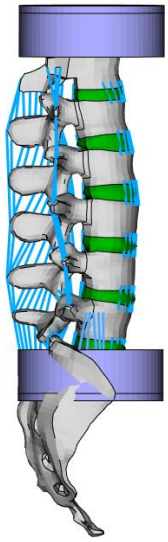

Figure 10. Repositioned spine to align with the seated soldier study by Reed et al. (2013), as tested by Ortiz-Paparoni et al. (2020).

.

3.3.2.3 Parametric study

A parametric study was conducted for the Ortiz-Paparoni simulation setup as the location of the upper potting cup (subjected to the cranial part of the lumbar spine) relative to the lower potting cup (subjected to the caudal part of the lumbar spine) was not specified in their work (Figure 11). Therefore, the center-to-center distance of the upper potting cup to the lower potting cup was predicted by comparing the spine stiffness obtained from the simulation setup and the spine stiffness obtained from the experiment. Table 3 displays six different positions of the upper platform center line that were simulated.

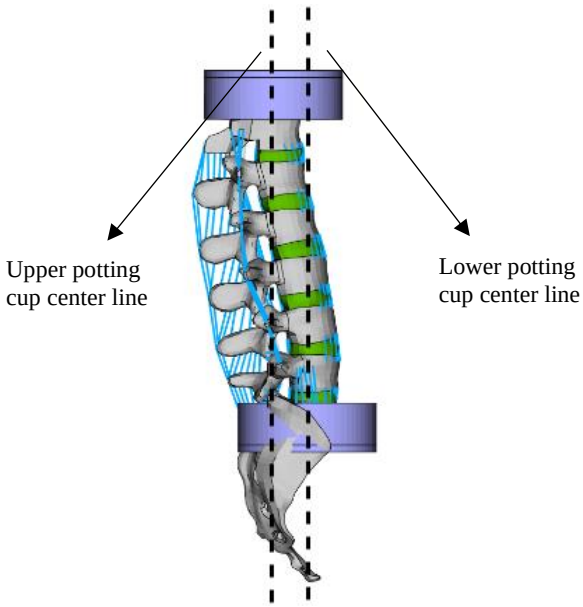

Figure 11: Location of the lower potting cup relative to upper potting.

Table 3. The parametric study corresponding positions labelled 1-6 and distance to the sagittal axis of the lumbar spine. Negative values of distance to the sagittal axis indicates the upper potting cup center line is moved posteriorly forward from the sagittal axis. Positive value indicates the upper potting cup center line is moved anteriorly forward.

Simulation	1	2	3	4	5	6
Distance to the sagittal axis (mm)	-24	-19	-14	-9	-4	1

3.4 Whole-Body Human Body Model Laboratory Sled Test Validation and THOR Comparison

The HBM laboratory sled test validation was based on a study conducted by Richardson *et al.*, (2020). The aim of this study was to evaluate the kinematic and injury response of reclined PMHS in 30 g, 50 km/h frontal sled tests. The study included five mid-sized adult male PMHSs. Richardson *et al.* (2020) used a semi-rigid seat with an anti-submarining seat pan and an experimental three-point seatbelt (triple pre-tensioned, force limited, seat integrated). They measured the global motions and local accelerations of the head, pelvis, and multiple vertebrae. Additionally, seat and seatbelt forces were measured. During the experiment, one of the five PMHS submarined, leading to its exclusion from the kinematics and kinetics results. Three of the five PMHS experience a lumbar spine fracture, all at the L1 vertebra. The objective of the whole-body validation was to assess the strain-based IRF proposed by Chalmers together with SAFER HBM v10X on a whole-body level.

A biofidelity evaluation of the Hybrid-III 50th male and the THOR-50M ATDs was conducted by Shin *et al*. (2022) in the same test setup as the PMHS test study. The objective of the study was to compare the kinematics of the Hybrid-III 50th male and THOR 50th male ATDs with that of PMHS. To achieve this, three tests were conducted per ATD in a reclined condition, like the one used in the PMHS testing. To establish a correlation and conduct a comparative analysis of the motion characteristics between vertebrae in PMHS and ATD, pseudo-anatomic points were introduced onto the ATD's structure. These points serve as representations of the PMHS vertebrae on the ATD's structure (Figure 12).

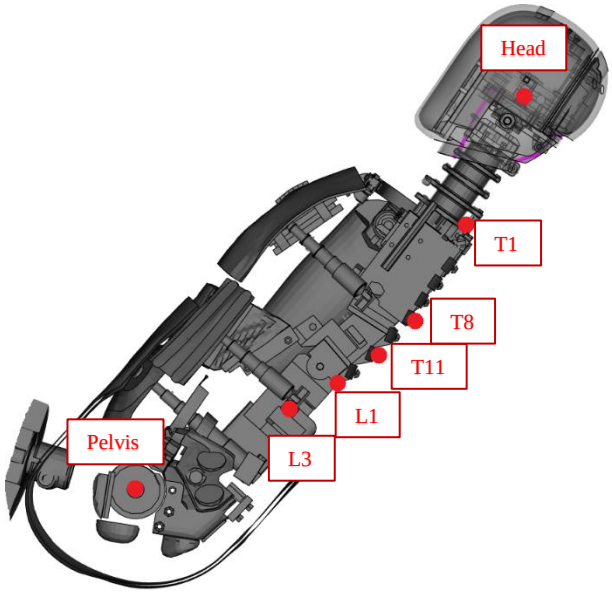

Figure 12. Location of the pseudo-anatomic points on THOR-50M.

3.5 HBM Laboratory Sled Test Simulation Setup

This section outlines the FE model of the sled as well as positioning and belt routing procedure of the HBM on the sled.

3.5.1 Sled Simulation Setup

The FE model used in the reclined, PMHS test study by Richardson *et al*., (2020) was designed to replicate the experimental setup, which consisted of a semi-rigid seat and a foot support, Figure 13, the seat pan angle was adjusted to achieve a 50° torso angle.The FE model was previously developed and used by Gepner *et al*., (2022), who conducted simulations of HBMs and sled to assess their kinematics in comparison to the PMHS test study. The acceleration pulse of 30-g (ΔV = 50 km/h) was applied to the sled (Figure 13). The semi-rigid seat was based on a design created by Uriot *et al.*, (2015) and the FE model of the seat was developed by the Laboratory of Accidentology and Biomechanics/Centre Européen d'Etudes de Sécurité et d'Analyses des Risques (LAB/CEESAR) in collaboration with the Partnership for Dummy Technology and Biomechanics (PDB). Autoliv Research further refined the FE-model.

In the FE setup as well as the PMHS test setup, an experimental restraint system was used that was developed to mitigate the likelihood of submarining in reclined sitting posture by Östling *et al*., (2017). It consists of 3-point belt with dual lap-belt pretensioners, a shoulder-belt retractor pretensioner with shoulder-belt load limiter set at 3.5 kN.

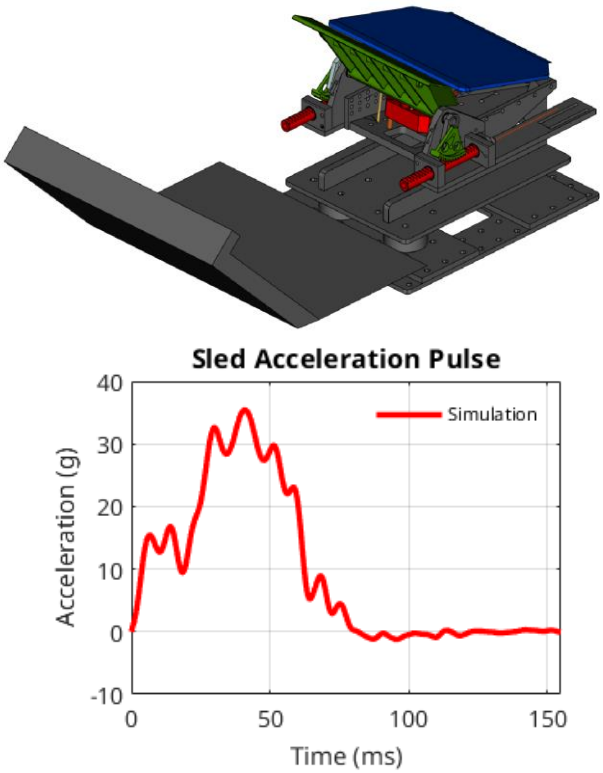

Figure 13. Finite Element Model of the Sled (top image) and the acceleration pulse (bottom image).

3.5.2 Human Body Model Positioning and Belt Routing

The 50th percentile male SAFER HBM v10 and v10X with the updated lumbar spine were both used in the simulation setup. The positioning of the V10X HBM was done in two steps. Initially, the H-point of the v10X was aligned with the average H-point of the PMHS, and subsequently, the position and angle of the HBM's pelvis were adjusted to match that of the PMHS, Figure 14. In the second step, the HBM was positioned based on the average position of L3, L1, T11, T8, T1, and the head of the PMHS (Figure 15). The positioning was achieved by using a displacement base cable approach in Oasys PRIMER (Arup, London, England), where the pelvis was constrained throughout the second step to maintain its rigid body alignment from previous step. Finally, to settle the HBM onto the seat pan, the seat pan was moved upwards to reach the desired depth of the buttocks and upper legs flesh compression while the HBM's skeleton was constrained, Figure 16, such that there would not be any rigid body motions of the HBM. The v10 HBM was positioned as in the previous study (Gepner *et al.* 2022).

Using belt routing algorithm in Oasys, the shortest path for the belt was formed by stretching the lap belt and chest belt across the model (Figure 16).

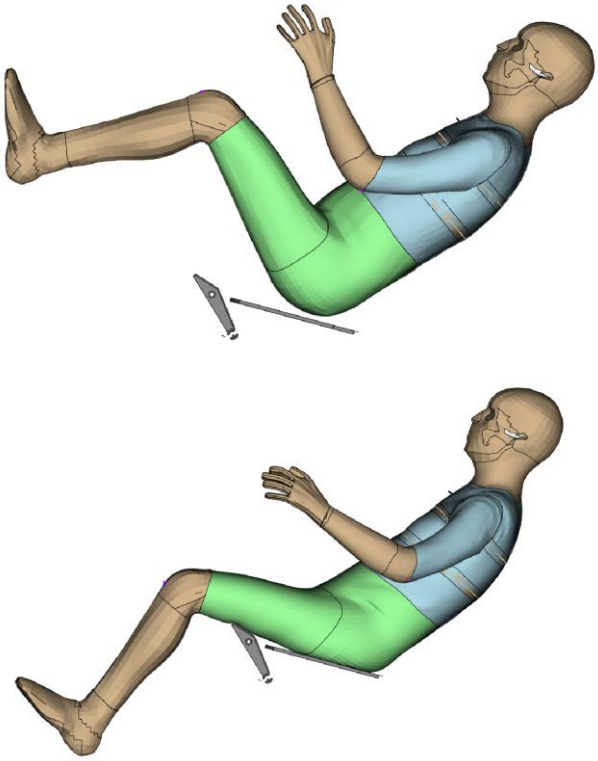

Figure 14. First step of positioning the HBM v10X (top image) and second step of positioning the HBM v10X (bottom image).

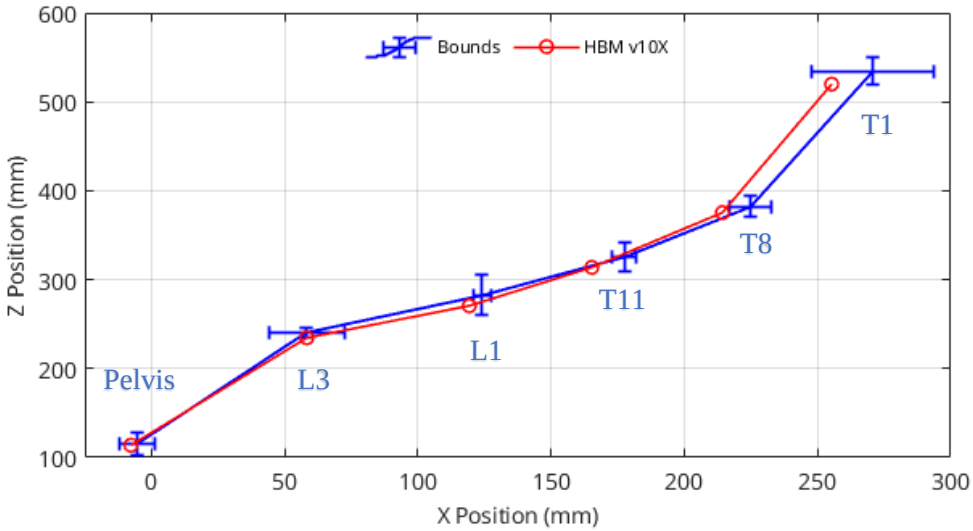

Figure 15. Position of the pelvis, L3, L1, T11, T8 and T1 from the SAFER HBM v10X compared with the test results from Richardson et al., (2020) in which they reported the average and the standard deviation of obtained from the positions of the five PMHS.

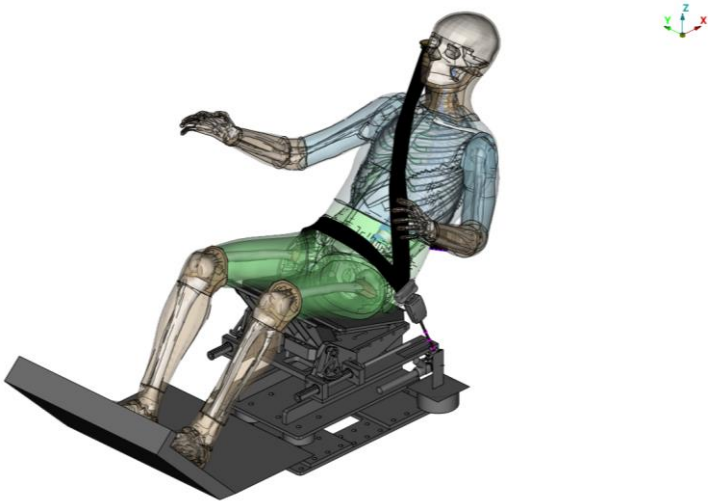

Figure 16. Final position of the HBM v10X on the sled.

3.6 THOR Laboratory Sled Test Simulation Setup

In this chapter, the FE model of the THOR-50M used in the simulation setup is studied. The sled, restraint system and the pulse were set up with the same configurations as those used in the HBM simulation setup.

3.6.1 THOR positioning and Belt Routing

To position the THOR in the same manner as in the test setup by Shin *et al.*, (2022), a series of consecutive steps were taken. Firstly, as the H-point of the THOR was not specified in the test setup, a trial-and-error procedure was undertaken to align the H-point as closely as possible with respect to the test setup. Additionally, the pelvis was rotated to a final value of 43° (Figure 17). In the second step, using a displacement base cable approach in Oasys PRIMER, the lower thoracic pitch was adjusted to achieve a sagittal torso angle of 48 degrees, and the upper and lower legs were positioned such that the feet are well placed on the foot support (Figure 17). Finally, to settle the THOR onto the seat pan, the seat pan was moved upwards to reach the desired depth of the lower torso pelvis flesh compression while the dummy's pelvis was constrained (Figure 18).

The belt routing was done with forming the shortest path, Figure 18, by stretching the lap belt and chest belt across the model in Oasys PRIMER.

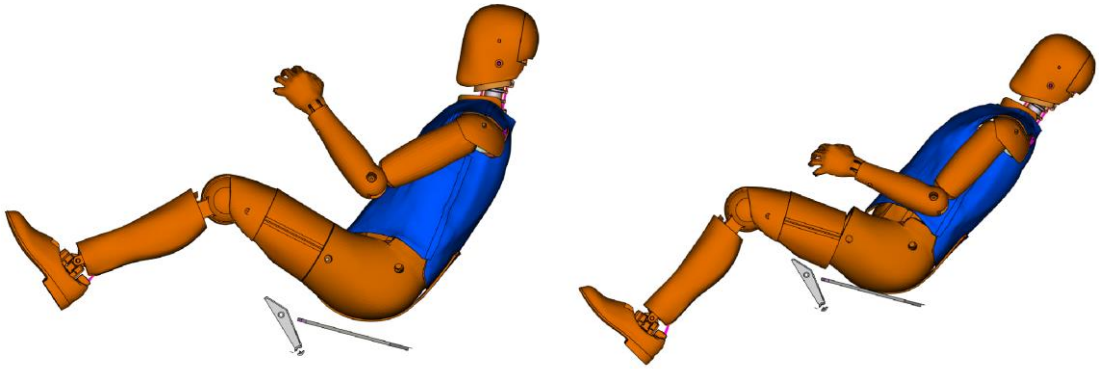

Figure 17. First step of positioning the THOR (left image) and second step of positioning the THOR (right image).

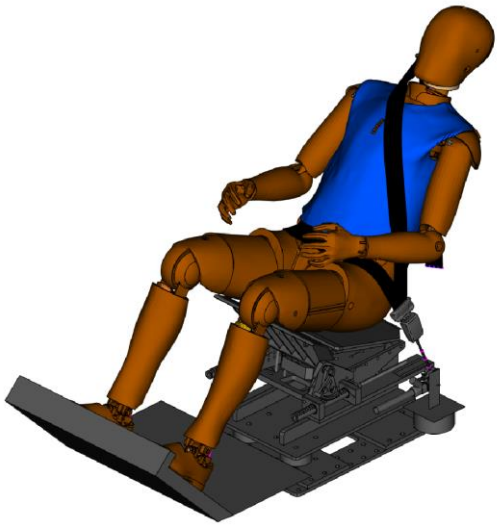

Figure 18. Final position of the THOR on the sled setup.

3.7 Accident Reconstruction Assessment

An accident reconstruction was simulated, based on real-world accident described by Jakobsson *et al.,* (2016) that occurred between a Volvo V40 (2014) and a Peugeot Bipper on a wet, rural road during the evening (Figure 19(a)). A restrained 44-year-old male was driving the Volvo V40, at approximately 80 km/h when the driver of the Peugeot Bipper, for unknown reasons drifted into his lane (Figure 19(b)). Before being impacted by the Peugeot Bipper, the driver of the Volvo used the brakes and reduced the speed by roughly 20 km/h. The angle of impact was about 10 degrees and an overlap of 80%, the estimated impact speed was 60 km/h for the Volvo and 80 km/h for the Peugeot. The driver of the Volvo sustained a moderate compression fracture on the L5 vertebra, reduced to approximately 50% of total height (Figure 19(c)). Furthermore, the driver of the Volvo sustained other moderate fractures. For instance, in his right ankle and left foot, yet sustained no injuries to his head or torso.

During the post-accident inspection, the driver's seat of the Volvo showed deformations on the seat chassis structure, slightly in front of his initial pelvis position. Even though the forces on the vehicle were predominantly longitudinal, Jakobsson *et al.*, (2016) suggested that the mechanism behind the lumbar compression spine fracture is axial load, transferred to his spine due to the pelvis interaction with the seat in combination

with the seatbelt interaction. The acceleration pulse of the impact was recorded in the Volvo V40 Event Data Recorder (EDR).

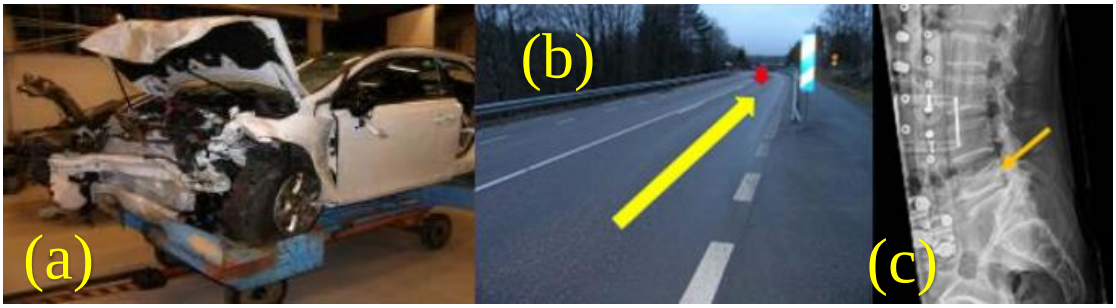

Figure 19. (a) Volvo V40 after the frontal impact. (b) Accident site. The long arrow indicated the position and direction of the Volvo V40. The short arrow indicated the position and direction of the Peugeot Bipper. (c) X-ray scan of the L5 compression fracture. Adapted from Jakobsson et al. (2016).

3.7.1 Accident Reconstruction Simulation Setup

The configurations of the FE model were based on previous work reported by Pipkorn *et al.*, (2019). Both SAFER HBM v10 and SAFER HBM v10X were positioned in the driver seat of the Volvo V40 driver compartment FE-model (Figure 20(a-b)). The recorded EDR pulse was applied to the driver compartment model and restraints were triggered at the same time as in the accident.

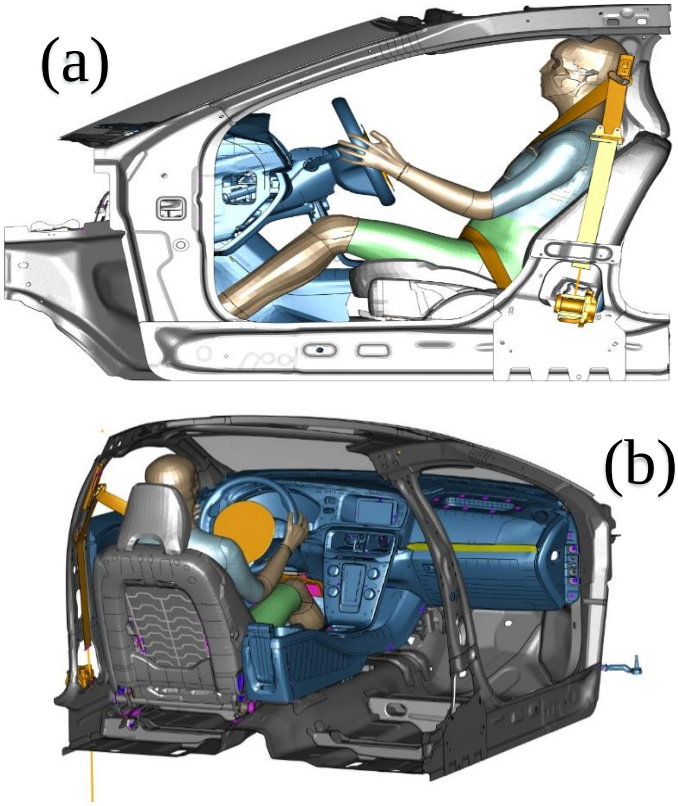

Figure 20. (a) Volvo V40 driver compartment FE-model with the SAFER HBM v10X positioned during the impact simulation from the side. (b) Volvo V40 driver compartment FE-model with SAFER HBM v10X positioned during the impact simulation from the back.

3.8 Post-processing Tools

A set of post-processing scripts which were implemented using META version 23.1.0 (Beta CAE Systems, Luzern, Switzerland) was used to extract peak strain values, compressive forces, bending moments and kinematics. Some of the scripts used MATLAB version R2019b (Mathworks, Nattick, MA) for further processing of data extracted from the LS-DYNA binary databases by META, for instance, to calculate the lumbar vertebra fracture risk. All the processed data was saved in comma separated text-files.

4 Results

All simulations reached the full simulation time (Normal termination). The isolated lumbar spine simulations were run on 60-72 CPU. For the laboratory sled test simulations, the SAFER HBM v10X were run on 120-140 CPU, while the SAFER HBM v10 were run on 120-128 CPU. The accident reconstruction simulations were run on 240-256 CPU.

4.1 Injurious Isolated Lumbar Spine Validation

The compressive cross section forces in L1 and L4, Figure 21, had similar peak compressive forces. However, the placement of the upper platform CoG had a large effect on the compressive peak forces in L1 and L4, giving a range of 3.9–5.5 kN in L1 and 4.1–5.9 kN in L4. The highest compressive peak forces in both L1 and L4 were found when the upper platform CoG was placed 2.3 cm anterior from the L2-L3 PLL axis. The lowest compressive peak forces in both L1 and L4 was when the upper platform CoG was placed farthest anteriorly from L2-L3 PLL axis. The simulation with 3.3 cm anterior offset was the closest to the reported point of contact between the upper platform and the cranial fixation in Stemper *et al*. (2018), Figure 5, with compressive peak forces in L1 of 4.5 kN and L4 5.0 kN. In addition, all the cross-sectional compressive forces from L1 to L4 are shown in Figure 33 in the Appendix.

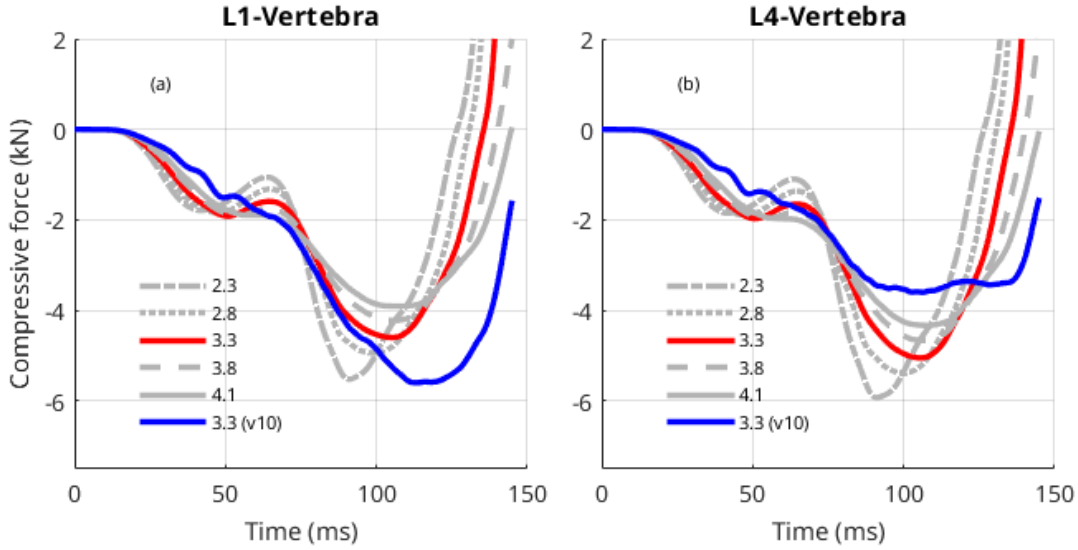

Figure 21. Time histories of the compressive cross section force in L1 (a) and L4 (b) vertebra for the different position of the Center of Gravity (CoG) of Rigid body 1 (upper platform). The legends correspond to the anterior offset from the L2-L3 PLL axis in centimeters and (v10) for the old lumbar spine FE model.

For the cross-section flexion moments of L1 and L4, Figure 22, the L1 spinal level exhibits greater flexion moments with a peak of 400 Nm compared with the L4 spinal levels peak of 50 Nm, for the V10X lumbar spine. However, the parameter study simulations showed a bending moment peak range in L1 between 135-400 Nm. Figure 22(a) show that the simulation configuration was sensitive to the applied load around 3.0-3.5 cm anteriorly from L2-L3 PLL axis, due to the relatively large bending moment peak. Moreover, the cross-sectional flexion moments from L1 to L4 are shown in Figure 34 in the Appendix.

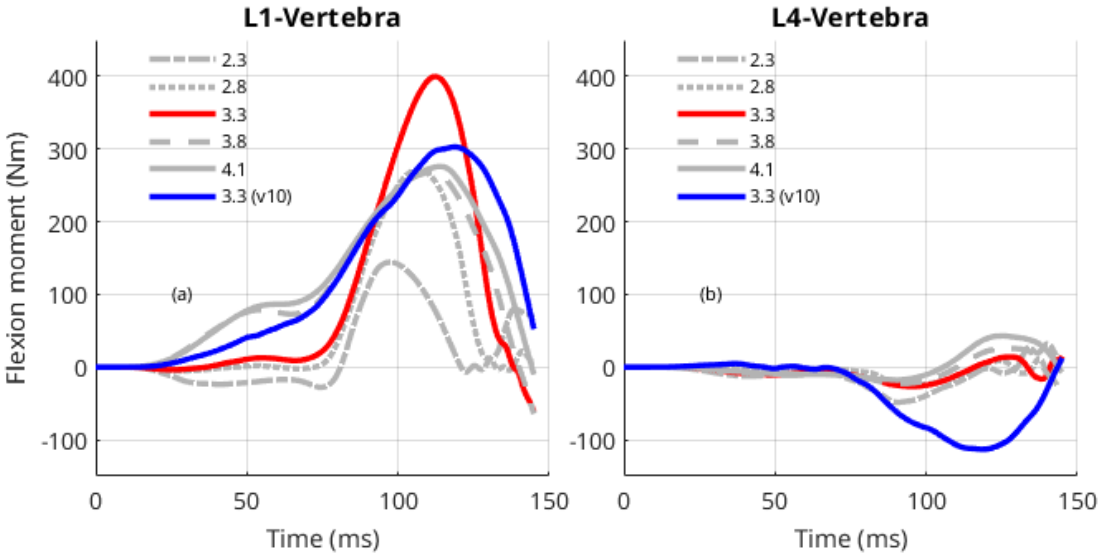

Figure 22. Time histories of the bending cross section moment in L1 (a) and L4 (b) vertebra for the different position of the center of gravity (CoG) of Rigid body 1 (upper platform). The legends correspond to the anterior offset from the L2-L3 PLL axis in centimeters and (v10) for the old lumbar spine FE model.

The load cell compressive cross-section forces, Figure 23, was sensitive to the placement of the upper platform CoG. Hence, the peak force range of the five parameter variations was between 5.0–6.2 kN. For this range of forces, the of lumbar vertebra fracture range according to IRF from Stemper *et al.* (2018), gives a range of 75–95% risk of fracture. The Simulation 3 peak force (5.7 kN), Figure 7, gives a risk of lumbar vertebra fracture about 90%. The proposed strain-based injury criteria by Chalmers gives a risk of lumbar vertebra fracture of a 50-year-old male from L1-L4 (39–98 %) for Simulation 3, Table 3.

Table 4. The risk of lumbar vertebra fracture and L_{index} values for a 50-year-old male in each vertebra from L1–L4, for Simulation 3 with 3.3 cm offset.

Injury Criteria	L1	L2	L3	L4
Chalmers (%)	98	96	65	39
Tushak (%)	100	100	100	100

Ortiz-Paparoni (%)	92	94	94	95
L_{index} (-)	3.2	2.6	1.7	1.2
Stemper (%)	53	65	65	67

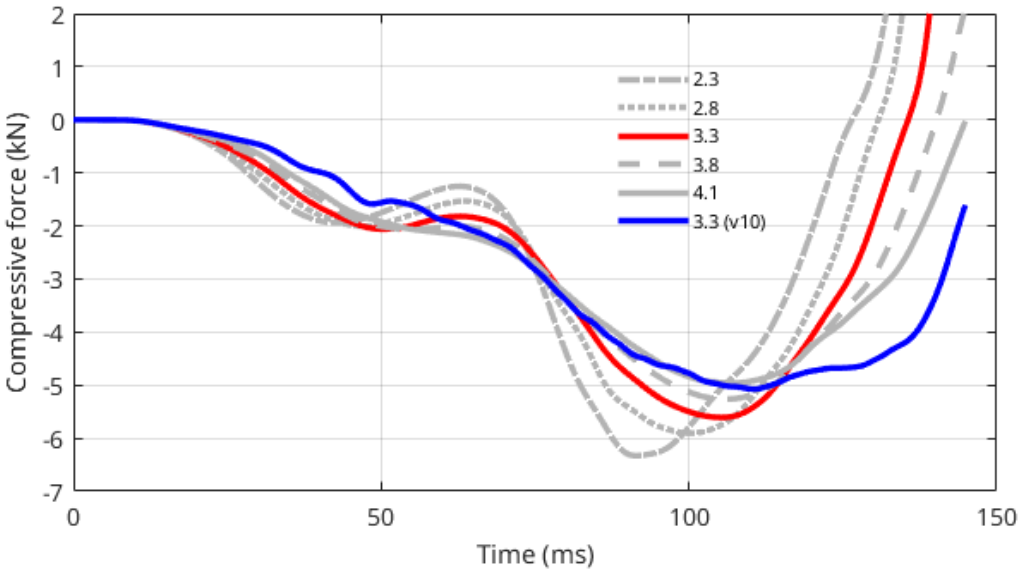

Figure 23. Time history of the load cell compressive cross section force. The legends correspond to the anterior offset from the L2-L3 PLL axis in centimeters and (v10) for the old lumbar spine FE model.

4.2 Non-Injurious Isolated Lumbar Spine Validation

The simulated lumbar response for the different position of the upper potting cup center line, (Figure 24), had a small effect on the stiffness of the lumbar spine. The resulting approximate linear stiffness range was between 272–282 N/mm. The stiffness of the lumbar spine increased as the upper potting cup center line was moved anteriorly forward.

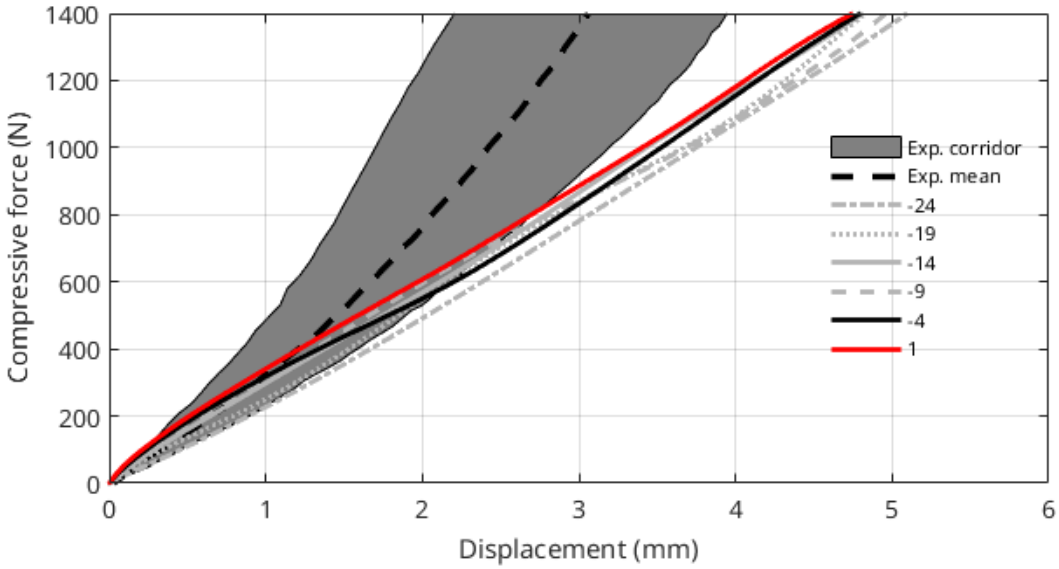

Figure 24. The simulated thoracolumbar response(stiffness) for the different position of the upper potting cup center line, during the loading. In comparison to the experimental thoracolumbar response in Ortiz-Paparoni et al. (2020).

The cross-sectional compressive forces during the applied load in L1 and L5, (Figure 25), had a small difference in terms of peak compressive force. L1 vertebra had a compressive peak force of approximately 1.5 kN meanwhile L5 vertebra had a compressive peak of 1.2 kN (Figure 25). However, some initial cross-sectional compressive forces were introduced by the pre-simulation to achieve the lumbar spine nominal posture of a seated soldier. For instance, 0.2 kN cross-sectional compressive force have been introduced in the L1 spinal level Figure 25. The compressive cross section force versus time in L1 (a) and L5 (b)-vertebra for Simulation 6, during the applied loading. loading, Figure 25(a)). The cross-sectional compressive forces from L1 to L5 during the dynamic loading are shown in Figure 35 in the Appendix.

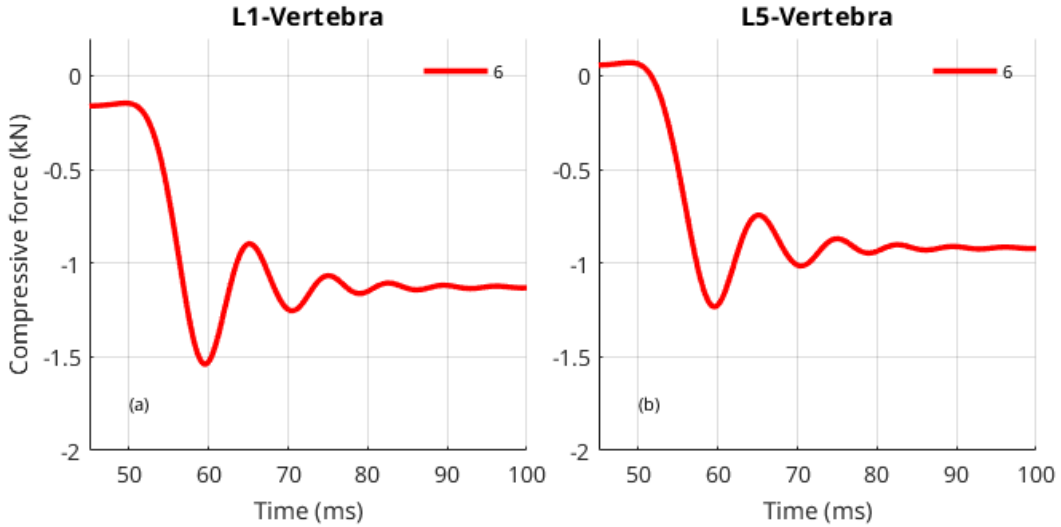

Figure 25. The compressive cross section force versus time in L1 (a) and L5 (b)-vertebra for Simulation 6, during the applied loading.

The cross-sectional flexion moments from L1 to L5 during the applied load under-body blast are shown in Figure 36 in the Appendix. The introduced cross-sectional flexion moment was found to be greater in L5 approximately 30 Nm, whereas in L1 it was 20 Nm (Figure 26).

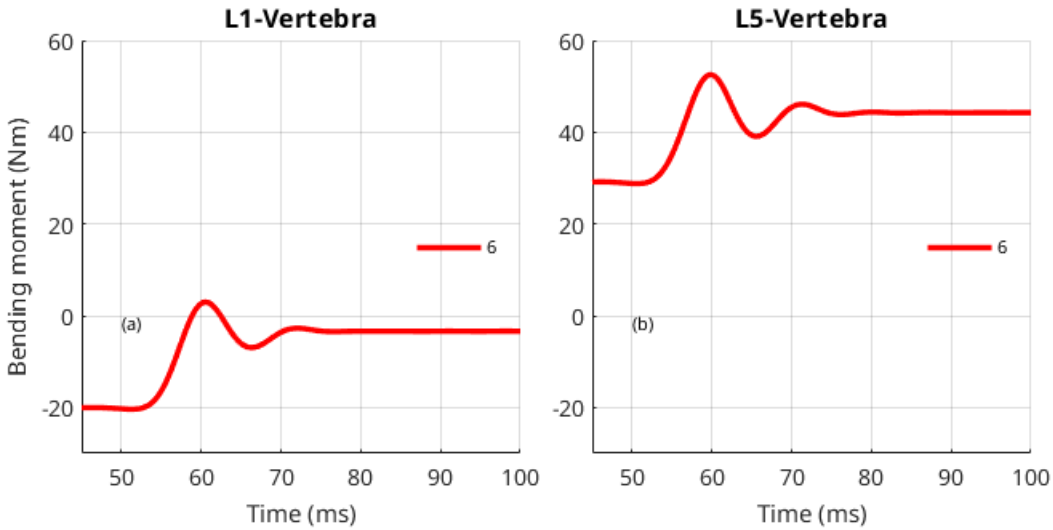

Figure 26. The bending cross section moment versus time in L1 (a) and L5 (b)-vertebra for Simulation 6, during the applied loading.

Tushak and Ortiz-Paparoni force-based IC yielded an insignificant risk of fracture, nearing zero, for the lumbar vertebrae ranging from L1 to L5. On the other hand, the Chalmers IC exhibited the highest fracture risk at L5 with a value of 3%, while the remaining lumbar vertebrae showed no risk of fracture.for a 50-year-old male. Low values of L_{index} were found, well below 1 for L1 to L5, Table 4.

Table 5. Simulation 6. The lumbar spine injury criteria for a 50-year-old-male in each vertebra from L1-L5.

Injury Criteria	L1	L2	L3	L4	L5
Chalmers (%)	0.0	0.0	0.0	0.0	3.40
Tushak (%)	0.1	0.1	0.0	0.0	0.0
Ortiz-Paparoni (%)	0.0	0.0	0.0	0.0	0.0
L_{index} (-)	0.46	0.42	0.39	0.45	0.56

4.3 Human Body Model Laboratory Sled Results

The kinematics, including the X and Z-displacements of T1, T8, T11, L1, L3, and pelvis of HBM v10X, were measured and compared with the test results (Figure 37 and Figure 38 in Appendix). Like previous results reported for the SAFER HBM v10 (Gepner *et al.* 2022), The kinematics of the SAFER HBM v10X aligned with the experimental corridors in the x-direction, although variations were observed in the z-direction. The kinematics are reported relative to the sled, which moved in the x-direction during the simulation.

The cross-sectional compressive forces and flexion moments of the SAFER HBM v10X at L1, L2, L3, L4, and L5 were measured and compared with those of the SAFER HBM v10. Moving from L1 to L5, there was a slight increase in the peak value in cross-sectional compressive forces with, L1 having the peak value at −4 kN and L5 at around

−4.8 kN. In contrast, the highest peak value in cross-sectional flexion moment was observed at L1 with a value around of 200 Nm, and it decreased as one moved towards L5 to a value of 100 Nm (Figure 39 and Figure 40 in Appendix). Although the compressive forces in HBM v10X and HBM v10 did not show any considerable difference, Figure 27, the cross-sectional flexion moment in vertebrae of HBM v10X was found to be greater in peak value than that in HBM v10 (Figure 28).

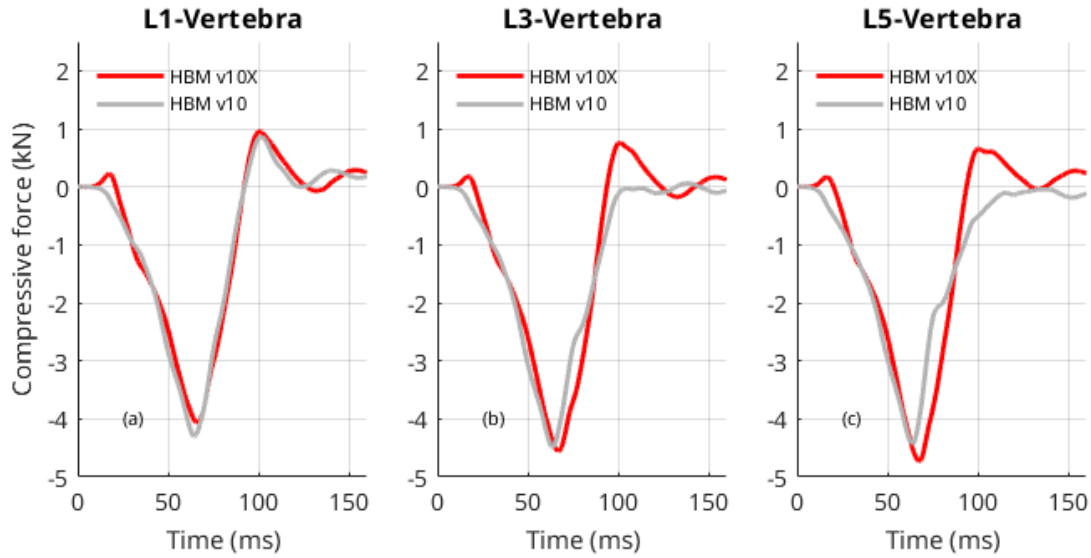

Figure 27. Time histories of the SAFER HBM v10 and v10X compressive cross section force in L1 (a), L3 (b) and L5 (c) vertebra.

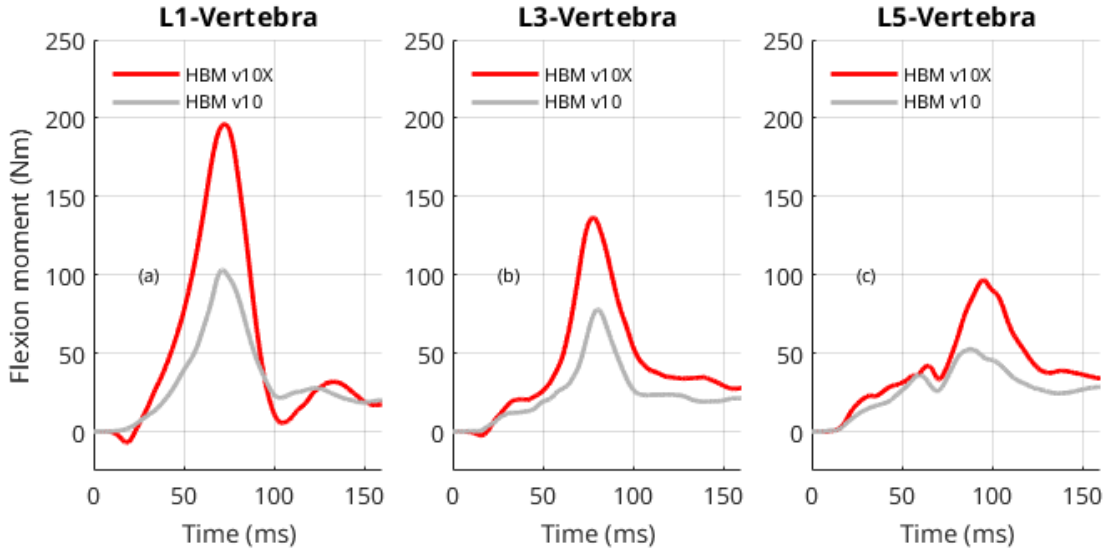

Figure 28. Time histories of the SAFER HBM v10 and v10X cross-sectional flexion moment in L1 (a), L3 (b) and L5 (c) vertebra.

For a comprehensive comparison between the FE model and the PMHS study, the Chalmers injury risk was determined for all the subjects, considering the different ages that Richardson *et al.* (2020) reported (Table 6). Given that the Tushak injury criterion also incorporates age as one of its parameters, for this analysis, where the focus was not on this specific injury criterion, the values are derived based on the average age of the subjects (54-year-old male). Based on the Chalmers strain-based injury criterion, the highest risk of fracture was observed at L1, while the lowest risk was at L4 for all the

subjects (Table 7). Nevertheless, the fracture risk obtained by Ortiz-Paparoni and Tushak indicates that the highest risk is observed at L2, with values of 27% and 28%, respectively. On the other hand, the lowest risk is observed at L4, with values of 22% and 17%, respectively (Table 7). The L_{index} IARV exceeded 1 in all vertebrae for both HBM v10X and HBM v10.

Table 6 The risk of lumbar vertebra fracture for the five subjects in PMHS study.

Injury Criteria	Test ID (Age)	HBM	L1	L2	L3	L4	L5
Chalmers (%)	S0529 (66)	v10X	97	89	76	57	61
		v10X	94	82	65	45	49
	S0530 (53)	v10X	98	92	80	62	66
		v10X	81	61	39	22	25
	S0531 (72)	v10X	94	83	67	47	50
	S0532 (25)						
	S0533 (55)						

Table 7 The risk of lumbar vertebra fracture for a 54-year-old male.

Injury Criteria	HBM	L1	L2	L3	L4	L5
Tushak (%)	v10X	28	28	15	17	19
	v10	25	23	12	14	14
Ortiz-Paparoni (%)	v10X	25	27	25	22	24
	v10	20	20	19	18	18
L_{index} (-)	v10X	2.0	1.9	1.8	1.6	1.6
	v10	1.5	1.5	1.4	1.4	1.3

4.4 THOR Laboratory Sled Results

The pseudo-points used on the ATD in this study correspond to specific anatomical landmarks such as the Head, T1, T8, T11, L1, L3 and Pelvis in the PMHS. The kinematic of the THOR FE-model was then compared with the findings from the research conducted by Shin *et al.* (2022) (Figure 41, Figure 42 and Figure 43 in Appendix). To evaluate the reliability of the seat belt FE model with the experiment, a comparison is made between the lap and shoulder belt forces derived from the FE model and the corresponding forces measured during physical tests (Figure 29). While the peak force in the FE model (9.4 kN) slightly exceeded the corresponding test results (8.5 kN) at approximately the same time, the overall recorded lap belt force demonstrated a close alignment with the expected range of values within the experimental corridor. The shoulder belt force in the FE model initially exhibited slightly higher values compared to the corresponding test result. From 50ms to 110ms, the force remained relatively

constant with the peak value of 3.2 kN and slightly lower than the test results that peaked at 4 kN, Figure 25.

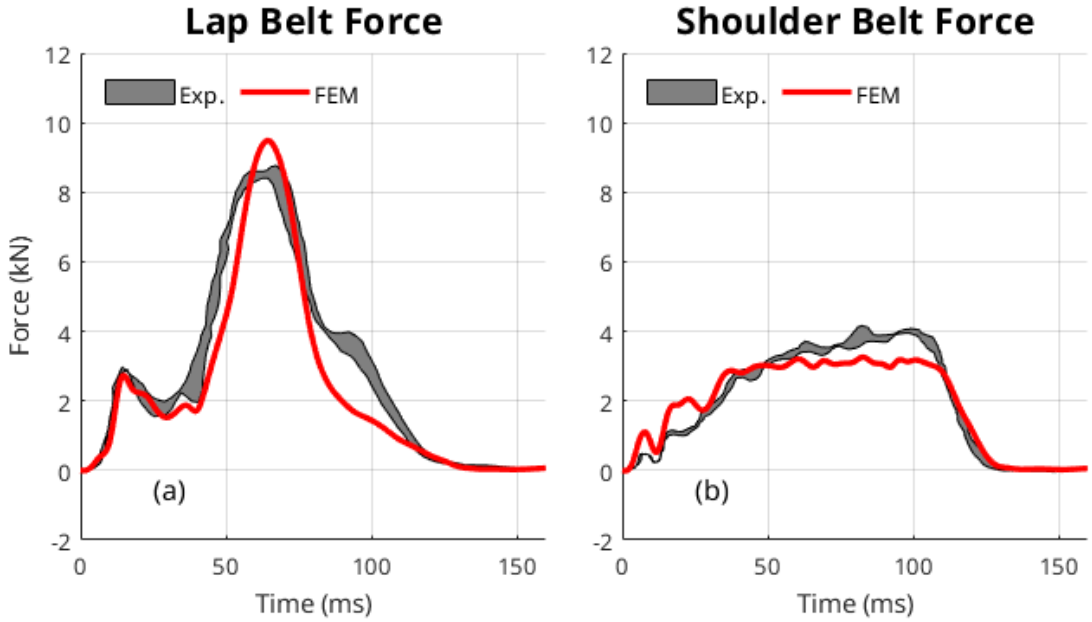

Figure 29. Lap and shoulder belt forces obtained from THOR sled simulation and compared with the test results of Shin et al. (2022).

The thoracic load cell (T12) compressive force and flexion moment were obtained for the THOR FE model and compared with the test result (Figure 30). The compressive force in the FE model exhibited lower values, reaching its minimum (−6 kN) slightly later than the test result, which had a minimum value of approximately −5.8 kN. Following the minimum, the force in the FE model increased gradually towards zero, whereas in the test results, it increased to a value of 4 kN before decreasing back to zero. The flexion in the thoracic observed in the FE model exhibited higher peak value of up to 600 Nm, occurring slightly later than the result, which peaked at 420 Nm.

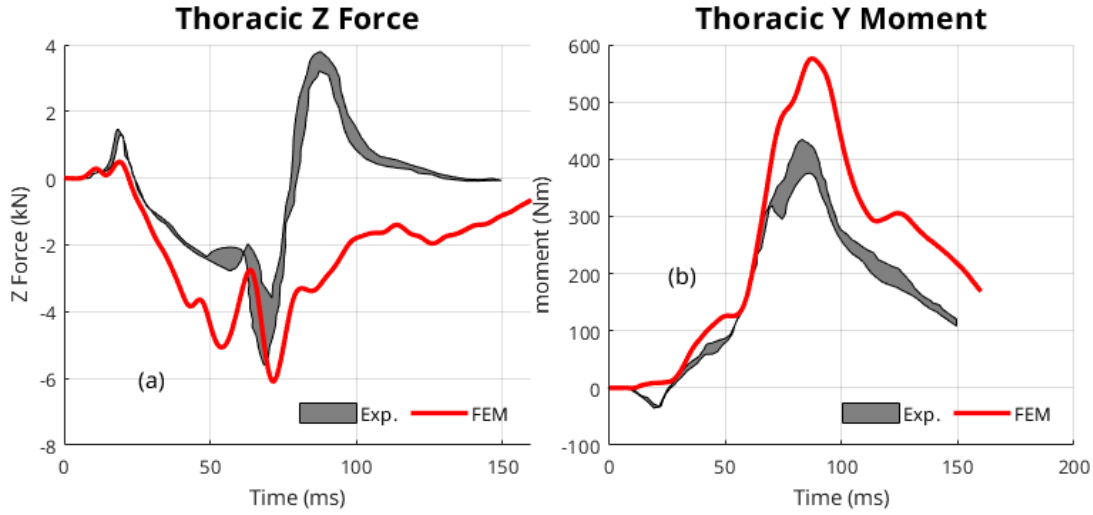

Figure 30. Thoracic compressive force and flexion moment obtained from THOR sled simulation and compared with the test results of Shin et al. (2022).

4.5 Accident Reconstruction Assessment

The cross-sectional compressive forces and flexion moments of HBM v10X were obtained at lumbar vertebrae and compared with those of HBM v10. The compressive force in HBM v10X at L1, L2, L3, and L4 were decreased to a peak value of −2 kN at around 65ms. At the same time as the other vertebrae, the compressive force in L5 was decreased to a peak value of −2.3 kN, which was later reduced to zero (Figure 31). Conversely, the flexion moment in HBM v10X had its highest peak value of 175 Nm at L5, gradually decreasing from L5 to L1 to a value of −20 Nm. The peak flexion moment occurs at approximately 70ms for all the vertebrae (Figure 32). For the SAFER HBM v10, the compressive force started with its lowest value of −2 kN at L1 and gradually increased from L1 to L5 to a value of −3.5 kN. Similarly, the flexion moment initially has its lowest peak at L1 and L2, measuring 24 Nm, and gradually increases to 70 Nm moving to L5. When comparing the cross-sectional compressive force and flexion moment between HBM v10X and HBM v10, it is evident that the peak value of compressive force was higher in HBM v10 across all vertebrae. Conversely, the peak value of flexion moment was higher in HBM v10X for all vertebrae (Figure 44 and Figure 45 in Appendix).

Injury risks were determined for a 44-year-old male involved in the accident (Table 8). According to the Chalmers strain-based injury criterion, the highest risk of fracture was observed at L5, measuring 68%, while the lowest risk was found at L2, measuring 4%. The Tushak and Ortiz-Paparoni force-based injury criteria showed relatively low fracture risks for HBM v10X, with maximum values of 1% and 2% at L5, respectively. Comparatively, the fracture risk increased for HBM v10 compared to HBM v10X based on the Tushak and Ortiz-Paparoni injury criteria. The L_{index} IARV exceeded 1 at L4 and L5 for HBM v10X and HBM v10.

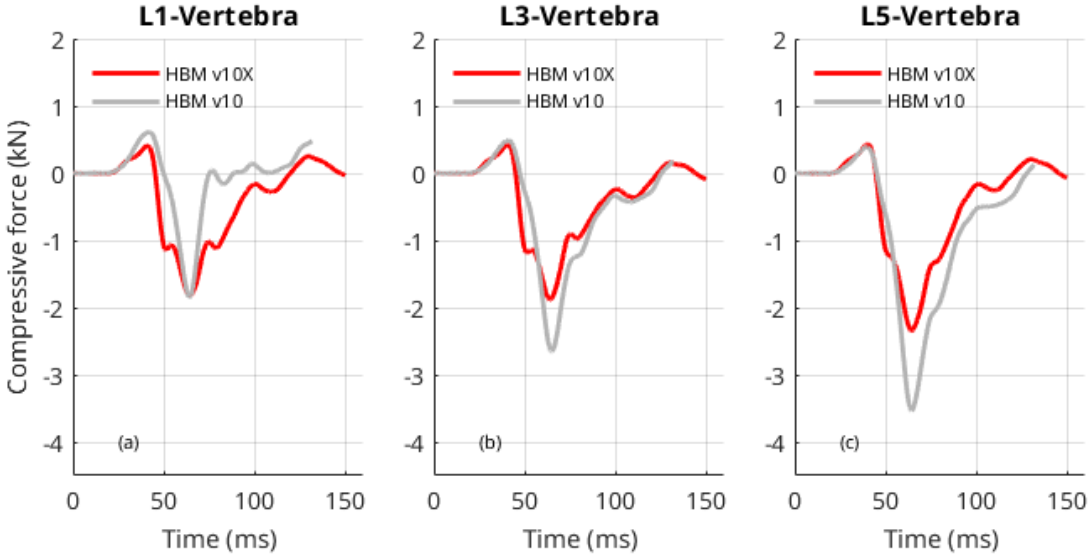

Figure 31. Time histories of the SAFER HBM v10 and v10X compressive cross section force in L1 (a), L3 (b) and L5 (c) vertebra.

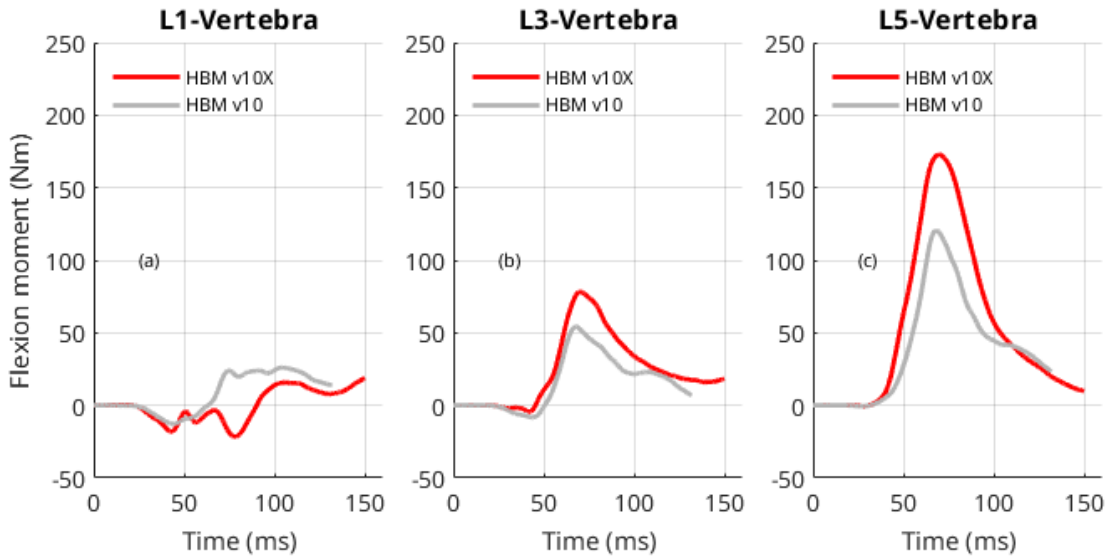

Figure 32. Time histories of the SAFER HBM v10 and v10X cross-sectional flexion moment in L1 (a), L3 (b) and L5 (c) vertebra.

Table 8. The risk of lumbar vertebra fracture for a 44-year-old male. N/A = Not Applicable.

Injury Criteria	HBM	L1	L2	L3	L4	L5
Chalmers (%)	v10X	25	4	30	54	68
	v10	N/A	N/A	N/A	N/A	N/A
Tushak (%)	v10X	0.2	0.3	0.2	0.5	1
	v10	0.2	0.4	0.8	3.6	5
Ortiz-Paparoni (%)	v10X	0.0	0.0	0.1	0.4	2
	v10	0.0	0.1	1.0	6.0	10.
L_{index} (-)	v10X	0.53	0.60	0.85	1.19	1.48
	v10	0.56	0.61	0.89	1.23	1.46

5 Discussion

Several reconstructions of Stemper *et al.* (2018) an injurious experiment, Ortiz-Paparoni *et al.* (2020) a non-injurious experiment, Richardson *et al*. (2020) whole-body laboratory sled test and accident reconstruction assessment were undertaken. Furthermore, the risk of lumbar spine fractures was estimated using a new tissue-based IC and IRF and compared with the experimental findings of the PMHS injuries. In addition, an attempt to compare the risk of injury obtained from the SAFER HBM v10X with measurements of THOR was explored.

5.1 Isolated Lumbar Spine Validation

The acceleration recorded in one of the experiments conducted by Stemper *et al.* (2018) was used as the boundary condition in the simulation setup. To assess the robustness of the FE model, the upper plate CoG was moved anteriorly along the sagittal axis relative a horizontal line from the L2-L3 Posterior Longitudinal Ligament (PLL). Since the description of the experimental setup explicitly indicated the absence of slippage between the upper plate and the superior potting cup fixation (Stemper *et al.* 2011), a revolute joint was implemented in the simulation setup to replicate the motion observed in the experimental configuration.

Based on the data obtained from the series of experiments conducted by Stemper *et al.* (2018), which included 17 specimens, peak forces were recorded using a load cell. Since only the acceleration response of a single case was reported in Stemper *et al.* (2011), the validation was conducted based on that specific case. The resulting peak forces obtained from the simulation setup ranged from of 5.0 to 6.2 kN, Figure 21, and were close to those reported which ranged from 4.7 to 6.7 kN.

A noticeable observation is that as the upper plate was moved anteriorly, the peak force decreased, which was expected as the force became more eccentric. However, the peak moment initially increased to 400 Nm and then decreased, Figure 22. The increase in the moment can be attributed to the application of an eccentric load, causing the spine to surpass its stability point, and become more prone to significant curvatures when subjected to smaller moments.

According to the Chalmers strain-based IC, the high fracture risk observed in L1 and L2 (Table 4) signifies high strain levels present in those specific vertebrae. Stemper *et al.* (2018) found that most injuries occurred at the L1 spinal level, indicating that Chalmers injury criterion can predict injurious loading conditions and accurately specify the spinal level of injury also for an isolated lumbar spine simulation. In contrast, IRF obtained by Ortiz-Paparoni was with the highest risk of injury at L4, with a decreasing trend moving from L4 to L1. In addition, the moment significantly increases while transitioning from L4 to L1, while the force only slightly decreases in the same order. This suggests that force has a more significant impact than flexion in Ortiz-Paparoni's injury criterion. The Tushak injury criterion showed a considerable risk of fracture in all vertebrae for the injurious simulation setup. On the other hand, the L_{index} IARV, which also incorporates both force and moment, had the highest value in L1. However, moving towards L4, the L_{index}decreased to its lowest value. This implies that the flexion moment is the dominant factor for L_{index} compared to the compressive force. The Stemper injury criteria, which only considers the compressive cross-sectional force, indicated that the highest fracture risk occurs at L4, while the lowest risk is at L1. This is because L4 experiences the highest cross-sectional force, gradually decreasing as we

move toward L1. However, since the Stemper injury criterion is based on a particular experimental setup and relies on cross-sectional forces measured by a load cell in that setup, it does not effectively determine the location of the spinal injury.

A non-injurious experiment conducted by Ortiz-Paparoni *et al.* (2020) was simulated to assess the Chalmers, Tushak and Ortiz-Paparoni force-based injury criterion to separate between injured and non-injured on an isolated lumbar spine level. Based on the result from the injury risk predictions for lumbar vertebra fracture of a 50-year-old male, Table 5, a significantly low fracture risk was found for both the Tushak and Ortiz-Paparoni force-based injury criteria across all vertebrae. Similarly, the Chalmers injury criterion indicated a low risk of injury at all vertebrae levels. Additionally, the L_{index} IARV did not surpass the fracture threshold for any vertebrae. These results suggest that the Chalmers injury criterion effectively differentiates non-injurious cases.

5.2 HBM Laboratory Sled Test Validation

Richardson *et al.* (2020) conducted a study which was used validate the SAFER HBM v10X which is the SAFER HBM v10 with newly developed FE model of the lumbar spine in whole-body laboratory sled test. They evaluated the kinematic and injury response of reclined PMHS subjects using a semi-rigid seat and a non-production three-point seatbelt. The FE model used in the study aimed to replicate the experimental setup and included a semi-rigid seat and foot support.

The PMHS study conducted by Richardson *et al.* (2020) reported that four out of five PMHSs experienced injuries to the sacral/coccygeal region. The combination of constrained pelvic and the inertia of the upper torso led to a flexion and compression effect on the lumbar spine, resulting in fractures exclusively at L1 for three out of five PMHSs, with no other reported lumbar spine fractures among the subjects. Submarining, however, occurred in only one subject. As the FE model did not sustain any submarining, it can be indicated that the structural integrity of the FE model aligns with the PMHS study. Nevertheless, it should be noted that fractures in the PMHS can occur before reaching the maximum load point in the lumbar spine. Therefore, the SAFER HBM cannot replicate these loads accurately due to the absence of element deletion at fracture sites.

Compared to previous studies conducted by Gepner *et al.* (2022), the kinematics of the HBM v10X in this study closely align with those of SAFER HBM v10. When comparing the kinematics of the FE model with the PMHS results, there was a noticeable similarity in the x-displacement of L1, L3, and the pelvis, indicating a relatively good agreement. The x-displacements of T1, T8, and T11 initially fell within the test result corridor until 75ms into the simulation; at this point, the HBM v10X exhibited larger x-displacement values beyond the expected corridor. However, the HBM v10X displayed a diverging response in z-displacement throughout the time history. The divergent responses observed in the FE model, particularly regarding x-displacement and z-displacement, can be attributed to the higher degree of thoracic spine flexion exhibited by the HBM v10X compared to the thoracic flexion in the PMHS.

The similarity in kinematics and curvature between the HBM v10X and HBM v10, along with the higher values of flexion moment observed in the HBM v10X, indicates

that the updated spine in the HBM v10X leads to a stiffer model in comparison to the HBM v10.

For the subjects who sustained injuries at L1, according to the PMHS study, a high risk of fracture was obtained by the Chalmers injury criterion. However, among the subjects with no injuries at the lumbar spine, one was the youngest subject (S0532) with a value of 81% Chalmers's risk of lumbar fracture, while the other subject (S0533) with a high risk of fracture, experienced submarining during the experiment, thus excluded as the structural integrity of this subject was compromised. Upon comparing the Chalmers criterion to the Tushak and Ortiz-Paparoni criteria, it was found that the Chalmers criterion had a higher risk of lumbar vertebra fracture. Moreover, in numerous simulations, the L_{index} IARV exhibited a propensity to exceed threshold by indicating that HBM v10X experienced fractures at L1, L2, L3, L4, and L5. The Tushak and Ortiz-Paparoni criteria all indicated an increased risk of fracture for HBM v10X compared to HBM v10, which can be attributed to the greater flexion moment in HBM v10X in comparison HBM v10.

5.3 THOR

Simulations with THOR in the laboratory sled model was conducted with the initial intention to develop a transfer function between measurements in THOR and the injury risk predicted by SAFER HBM v10X. Therefore, the THOR ATD FE model was employed in a sled setup that was identical to the setup used for the HBM. The THOR simulation was implemented based on another experimental study (Shin *et al.* (2022) which compared the Hybrid-III 50th male and THOR-50M ATDs using the same setup as the PMHS test study.

When comparing the kinematics of the THOR FE model to the experimental results conducted by Shin *et al.* (2022), there is a noticeable alignment observed in the X displacement, Figure 41 to Figure 43. However, a significant disparity arises in the Z displacement. The FE model and experimental results for lap and shoulder belt force matched well, which indicates that the belt routing was done accurately. However, there was a significant disparity in the FE model's representation of the Thoracic Z force and Y moment with the experiment results. Therefore, to assess the reliability of the THOR-sled FE model, two additional H-point positions of the THOR were simulated. By examining these variations in the position of the THOR dummy on the sled, it was observed that even minor adjustments to the H-point position result in considerable changes in the Thoracic Z force and Y moment (Figure 46 in Appendix). The Thoracic Z force exhibited two distinct peak forces during the sled simulation, occurring at different locations of the THOR dummy. The first peak force, observed at approximately 50ms, occurred for Position 1 when the THOR began sliding on the seat pan. The second peak force, observed around 70ms, occurred when the THOR contacted the submarining pan. When comparing the Z force for different positions, it is evident that the first peak for Position 3 occurred earlier than the others, while for Position 2, the second peak occurred earlier than the others. These results suggest that the THOR dummy in Position 3 was positioned further away from the anti-submarining pan, while in Position 2, it was closer to the submarining pan. These findings indicate that the outcomes are highly influenced by the initial H-point position of the THOR dummy, and the discrepancy may be attributed to an excessively rigid sled. As a result, it was concluded to not be fruitful to try to compare the IRF values obtained from the HBM with lumbar spine measurements derived from the FE model of THOR in the

specific sled configuration. Consequently, no further comparison was made between the HBM and THOR in this context.

5.4 Accident Reconstruction Assessment

The quality of the accident reconstruction assessment is not great since it is based on a single case. Nonetheless, the simulated accident reconstruction was a good case to apply the Chalmers injury criterion on. Therefore, the driver of the Volvo V40 suffered a well-defined compression fracture at the L5 vertebra. The FE-model configuration used in the reconstruction is derived from previous work conducted by Pipkorn *et al.*, (2019). Where this configuration has undergone an iterative process and has been meticulously refined to closely align with the real-world accident. During the accident reconstruction, both SAFER HBM v10 and v10X models exhibited the same deformations on the seat chassis structure, positioned slightly ahead of the initial pelvis location. Which is believed by Jakobsson *et al.*, (2016) to have caused the compression fracture at L5 in combination with the occupant restraint system. This observation strongly indicates that the interaction between the occupant and the restraint system was very well reproduced. The result from the accident reconstruction and using the Chalmers injury criterion yields promising predictions regarding the risk of injury in this scenario, hence the highest risk of injury at L5, Table 8.

When comparing the results of the evaluated injury criteria for the accident reconstruction, it was found that Tushak and Ortiz-Paparoni force-based IC did predict a low risk of lumbar spine fracture, Table 8. Conversely, the Chalmers injury criterion indicated a high risk of fracture (around 70%), at L5, which aligns with the actual fracture occurrence in the real-world accident. The possible explanation could be that Tushak and Ortiz-Paparoni criteria exhibit low sensitivity to the flexion moment, due to their high moment intercept values. On the other hand, the L_{index} IARV demonstrated its conservative nature in fracture prediction by exceeding the fracture threshold not only for L5 but also for L4.

The higher fracture risks obtained from Tushak and Ortiz-Paparoni force-based injury criteria for HBM v10, compared to HBM v10X, can be attributed to HBM v10 experiencing higher compressive forces, which is the dominant factor considered in these injury criteria.

5.5 Future Work

As a potential direction for future research in similar studies, it would be beneficial to simulate and validate additional cases from Stemper *et al.* (2018) experiments, considering each lumbar spine case possesses a unique acceleration pulse.

It would be valuable to simulate and validate experiments involving both injurious and non-injurious conditions on the isolated lumbar spine to further evaluate the predictive capacity of the Chalmers injury criterion.

Since the sled setup utilized in this study was not suitable for directly comparing the IRF obtained from the HBM and THOR measurements, it is recommended to explore alternative setups with lower stiffness, such as car FE models. These alternative setups could perhaps be more useful to establish a meaningful comparison between the HBM and THOR.

6 Conclusion

The predictive capacity of a recently proposed strain-based IC and its associated IRF for predicting lumbar vertebra fracture using a FE HBM was evaluated by comparing predicted fracture risks and actual number of fractures in experiments on PMHSs. Additionally, a study was undertaken to assess if the injury risk from the HBM could be related to measurements obtained from an FE model of the frontal impact ATD THOR.

The strain-based Chalmers IC and IRF demonstrated effectiveness in distinguishing between injured and non-injured cases in isolated lumbar spine simulations. In addition, this IC successfully predicted fractures in both isolate lumbar spine and whole-body level simulations, while the Tushak and Ortiz-Paparoni force and moment-based injury criteria were only effective in the isolated lumbar spine simulations. When these criteria were applied to whole-body simulations, they were unable to accurately replicate the experimental or real-life results due to their low sensitivity to the flexion moments. The L_{index} IARV demonstrated a tendency to exceed its threshold in numerous simulations indicating it is too conservative for the 50^{th} percentile male.

Due to the substantial impact of variations in the H-point position on the THOR-sled FE model, the comparison between the predictions of the FE HBM and the IRF with the lumbar spine measurements obtained from the FE model of THOR in this specific sled configuration was not feasible. Therefore, no comparison was made between the FE HBM and the THOR.

7 References

Begeman PC, King AI, Prasad P (1973). Spinal Loads Resulting from –Gx Acceleration. *Proceedings of Stapp Car Crash Conference*. SAE Technical Paper 730977, *Society of Automotive Engineers*, Warrendale, PA.

Belwadi A, Yang K (2008). Response of the Cadaveric Lumbar Spine to Flexion with and without Anterior Shear Displacement, *Proc. of the IRCOBI conference*, Bern, Switzerland, 397-410

Belytschko T, Liu WK, Moran B, Elkhodary KI (2014): *Nonlinear Finite Elements for Continua and Structures*, Second Edition

Duma S, Kemper A, McNeely D, Brolinson P, Matsuoka F (2006). BIOMECHANICAL RESPONSE OF THE LUMBAR SPINE IN DYNAMIC COMPRESSION. *Biomedical Sciences Instrumentation* 42: 476–481.

Gepner BD, Perez-Rapela D, Ostling, M, Pipkorn B, Forman J, Kerrigan JR (2022). Evaluation of GHBMC, THUMS and SAFER Human Body Models in Frontal Impacts in Reclined Postures. *Proc. of the IRCOBI conference*, Porto, Portugal, 116 – 143

Humanetics. (2020). *THOR-50M U.S. NCAP Dummy Model LS-DYNA Release Version 1.7.* Farmington Hills, MI, USA: Humanetics

Iraeus J, Niranjan Poojary Y, Jaber L, John J, Davidsson J (2023). A new open-source finite element lumbar spine model, its tuning and validation, and development of a tissue-based injury risk function for compression fractures. *Proc. of the IRCOBI conference*, Cambridge, UK

Jakobsson L, Björklund M, Westerlund A (2016). Thoracolumbar Spine Injuries in Car Crashes, *Proc. of the IRCOBI conference*, Malaga, Spain, 101-112

Klein C. and Davidsson J. (2023) SAFE-UP Report D5.5 Occupant models, https://www.safe-up.eu/prof/#WP5

Larsson, K. J., Pipkorn, B., Iraeus, J., Forman, J., & Hu, J. (2022). Evaluation of a diverse population of morphed human body models for prediction of vehicle occupant crash kinematics. *Computer Methods in Biomechanics and Biomedical Engineering*, *25*(10), 1125-1155.

National Highway Traffic Safety Administration (NHTSA). (2019). Newer Cars Are Safer Cars. Newer Cars Are Safer Cars | NHTSA

Ortiz-Paparoni M, Pigue M, Bass CR (2020). Building a Whole Spine from Segments: Lumbar Spine Response During Dynamic Compression. *Proc. of the IRCOBI conference*, Munich, Germany, 770-781

Ortiz-Paparoni M, Op't Eynde J, Kait J, Bigler B, Shridharani J, Schmidt A, Cox C, Morino C, Pintar, F, Yoganandan N, Moore J, Zhang JY, Bass C (2021). The Human Lumbar Spine During High-Rate Under Seat Loading: A Combined Metric Injury Criteria. *Ann Biomed Eng 49*, 3018–3030

Östling M, Larsson A (2019). OCCUPANT ACTIVITIES AND SITTING POSITIONS IN AUTOMATED VEHICLES IN CHINA AND SWEDEN. *Conference: The 26th International Technical Conference on the Enhanced Safety of Vehicles (ESV)*, Eindhoven, Netherlands, 19-0083

Östling M, Sunnevång C, Svensson C, Kock HO (2017). Potential future seating positions and the impact on injury risks in a Learning Intelligent Vehicle (LIV*). VDI-Tagung Fahrzeugsicherheit*, Berlin, Germany.

Pintar, FA, Yoganandan, N, Maiman DJ, Scarboro M, Rudd, RW (2012). Thoracolumbar Spine Fractures in Frontal Impact Crashes. *Annals of advances in automotive medicine. Association for the Advancement of Automotive Medicine. Annual Scientific Conference* 56: 277–283.

Pipkorn B, Iraeus J, Björklund M, Bunketorp OB, Jakobsson L. (2019). Multi-Scale Validation of a Rib Fracture Prediction Method for Human Body Models. *Proc. of the IRCOBI conference,* Florence, Italy, 175-191

Pipkorn B, Östh J, Brynskog E, Larsson E, Rydqvist L, Iraeus J, Perez-Rapela D, Jakobsson L. (2021). Validation of the SAFER Human Body Model Kinematics in Far-Side Impacts. *Proc. of the IRCOBI conference,* Online, 444-476

Reed MP, and Ebert SM. The seated soldier study: posture and body shape in vehicle seats. (2013)

Richardson Rachel, Donlon J, Jayathirtha M, Forman, J, Shaw G, Gepner, B, Kerrigan J, Östling, M, Mroz, K, Pipkorn B (2020). Kinematic and Injury Response of Reclined PMHS in Frontal Impacts. *Stapp Car Crash Journal* 64:83-153

Schmitt, K., Niederer, P. F., Cronin, D. S., Morrison III, B, Muser, M. H, Walz, F. (2019): *Trauma Biomechanics: An Introduction to Injury Biomechanics*

Shin J, Donlon J, Richardson R, Gepner, B, Forman J, Östling M, Kerrigan J (2022). Biofidelity Evaluation of the Hybrid-III 50th Male and the THOR-50M in Reclined Frontal Impact Sled Tests. *Proc. of the IRCOBI conference,* Porto, Portugal, 309-331

Stemper BD, Chirvi S, Doan N, Baisden JL, Maiman DJ, Curry WH, Yoganandan N, Pintar FA, Shender BS, Paskoff GR (2018). Biomechanical Tolerance of Whole Lumbar Spines in Straightened Posture Subjected to Axial Acceleration. *Journal of Orthopaedic Research* 36(6):1747 – 1756

Stemper BD, Storvik SG, Yoganandan N, Baisden JL, Fijalkowski RJ, Pintar FA, Shender BS, Paskoff GR (2011). A New PMHS Model for Lumbar Spine Injuries During Vertical Acceleration. *Journal of Biomechanical Engineering* 133(8):081002, https://doi.org/10.1115/1.4004655

Tushak S, Gepner B, Forman J, Hallman J, Pipkorn B, Kerrigan J (2022) Human Lumbar Spine Injury Risk in Dynamic Combined Compression and Flexion Loading.

Uriot J, Potier P, Baudrit P, Trosseille X, Petit P, Richard O, Compigne S, Masuda M, Douard R (2015). Reference PMHS Sled Tests to Assess Submarining (No. 2015-22-0008). SAE Technical Paper

World Health Organization. (2018, January). *Global status report on road safety*. Global status report on road safety 2018 (who.int)

Yoganandan, N., Moore, J., et al. Human lumbar spinal column injury criteria from vertical loading at the base: Applications to military environments. *Journal of the Mechanical Behavior of Biomedical Materials*, 2020: p. 103690

Zheng J, Tang L, Hu J (2017). A Numerical Investigation of Risk Factors Affecting Lumbar Spine Injuries Using a Detailed Lumbar Model. *Hindawi Applied Bionics and Biomechanics Journal*

8 Appendix

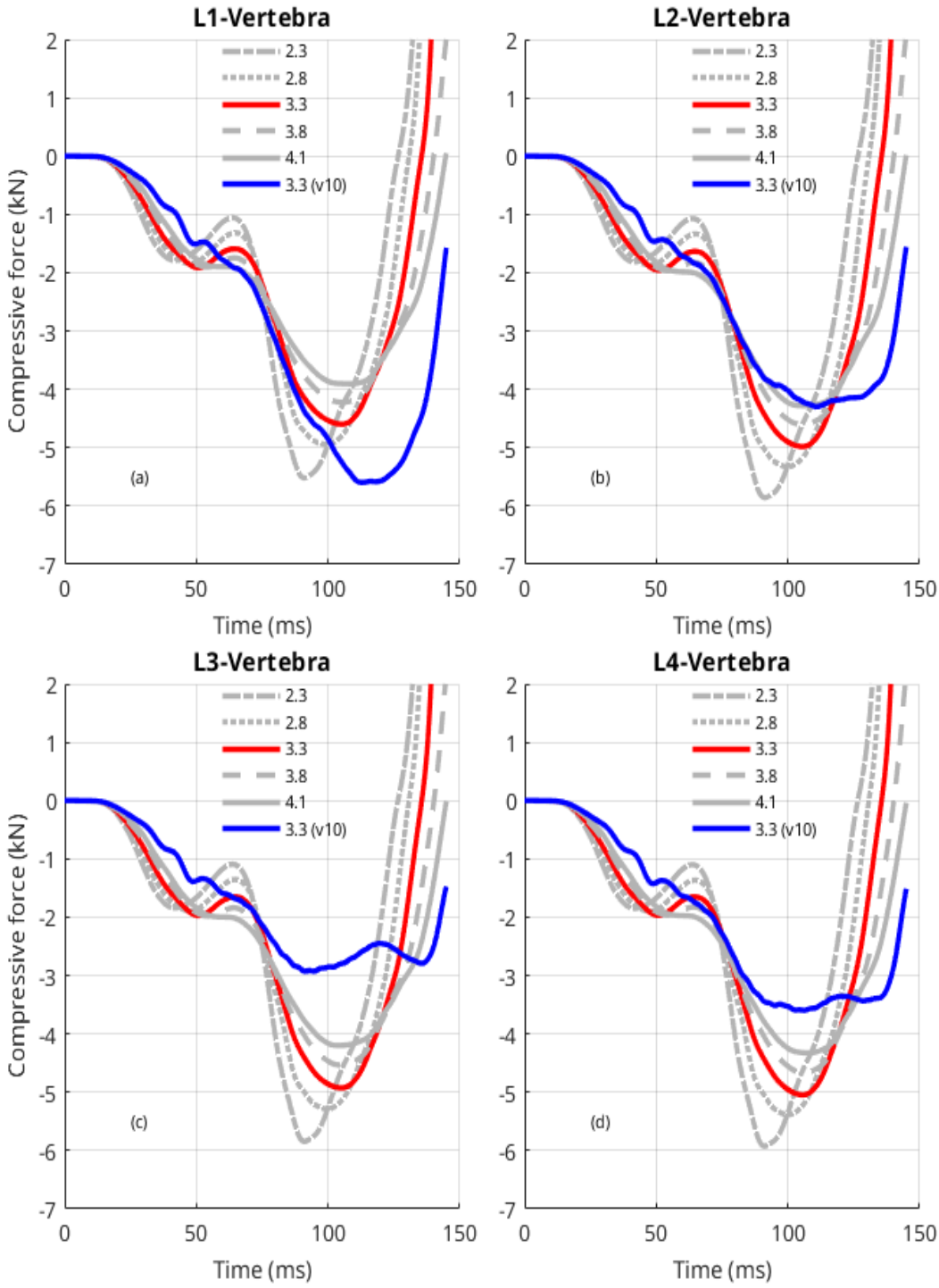

Figure 33. Time histories of the compressive cross section force in L1 (a), L2 (b), L3 (c) and L4 (d) vertebra for the different position of the center of gravity (CoG) of Rigid body 1 (upper platform). The legends correspond to the anterior offset from the L2-L3 PLL axis in centimeters and (v10) for the old lumbar spine FE model.

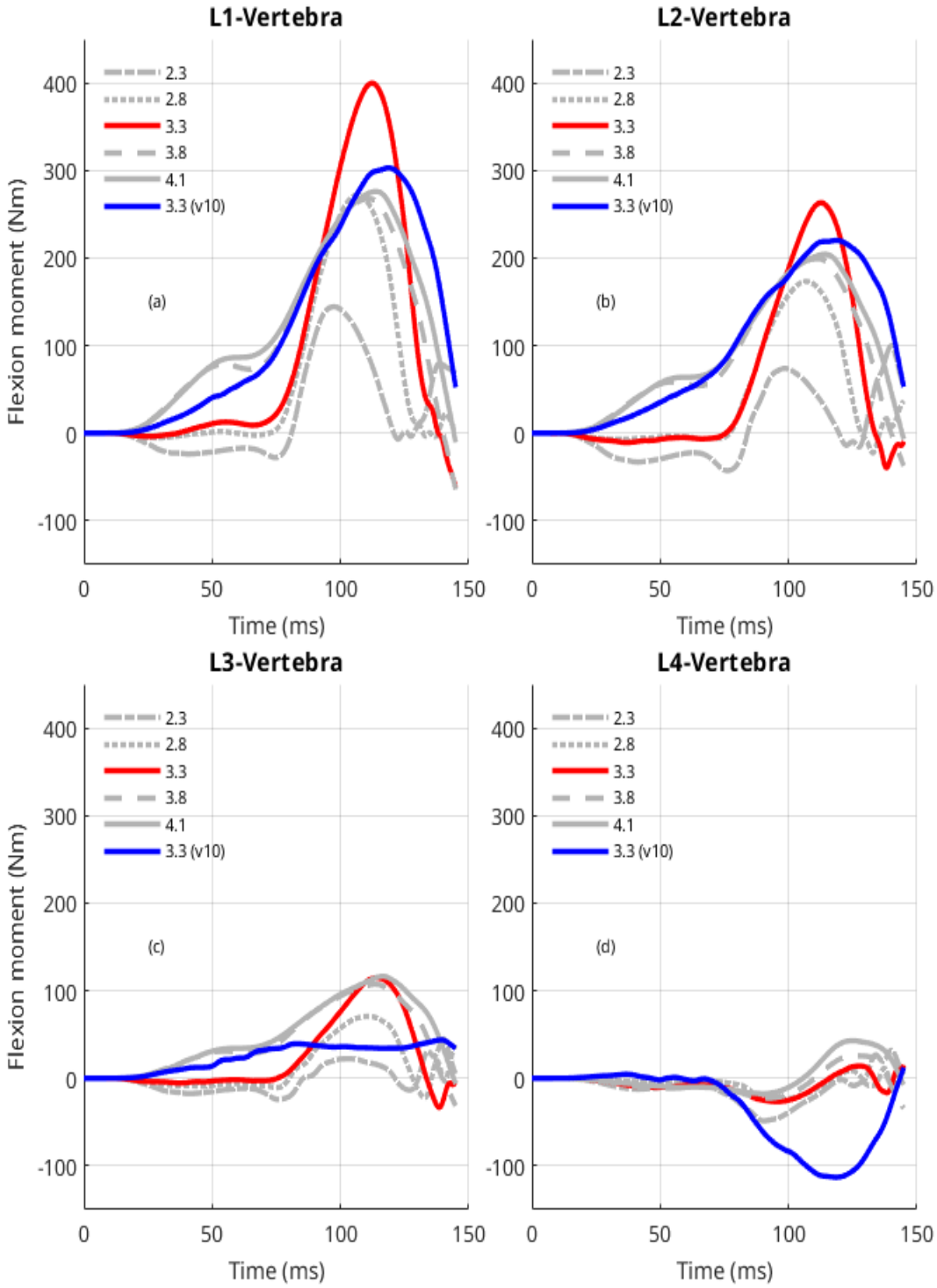

Figure 34. Time histories of the bending cross section moment in L1 (a), L2 (b), L3 (c) and L4 (d) vertebra for the different position of the center of gravity (CoG) of Rigid body 1 (upper platform). The legends correspond to the anterior offset from the L2-L3 PLL axis in centimeters and (v10) for the old lumbar spine FE model.

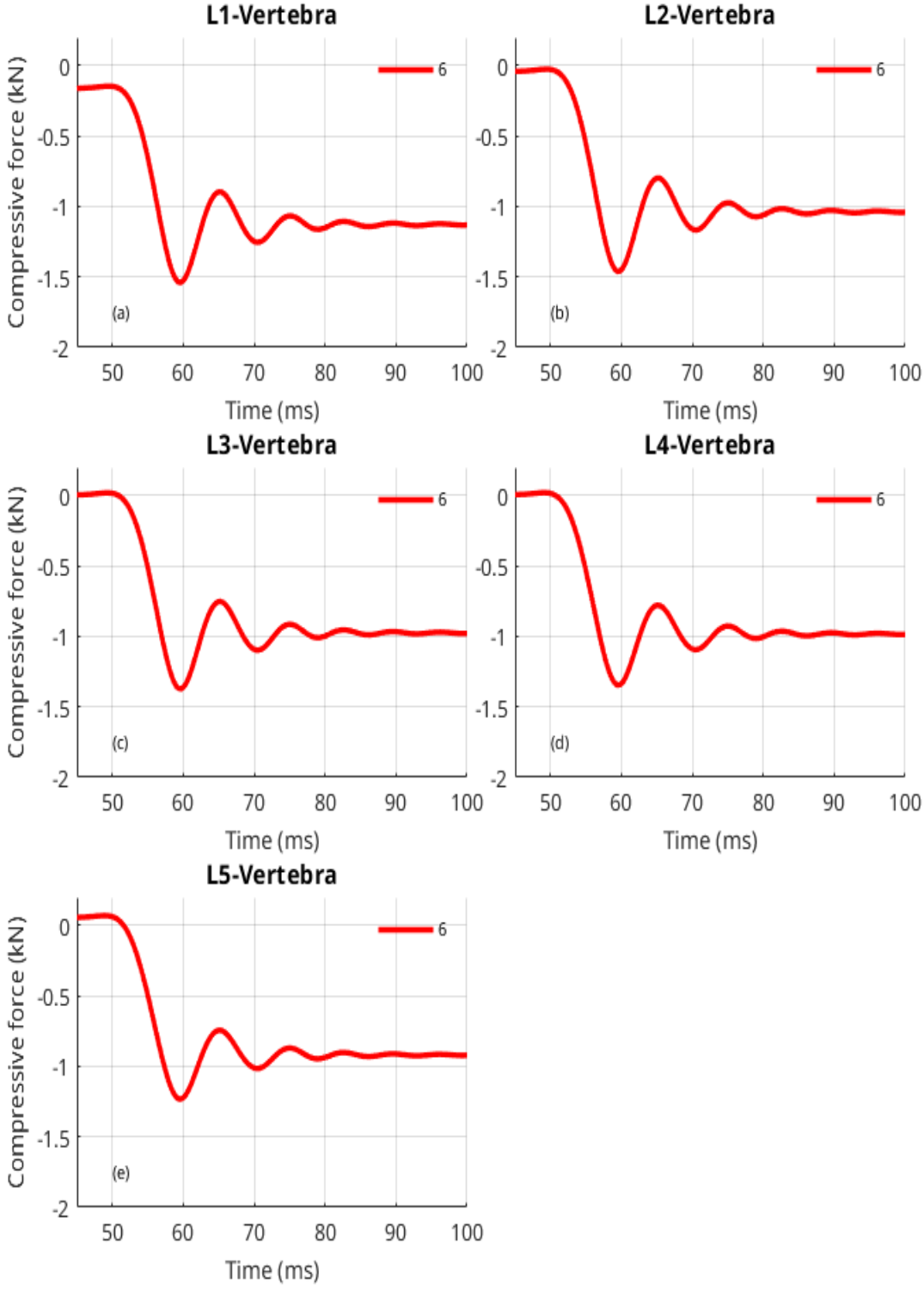

Figure 35. The compressive cross section force versus time in L1 (a), L2 (b), L3 (c), L4 (d) and L5 (e)-vertebra, during the applied loading.

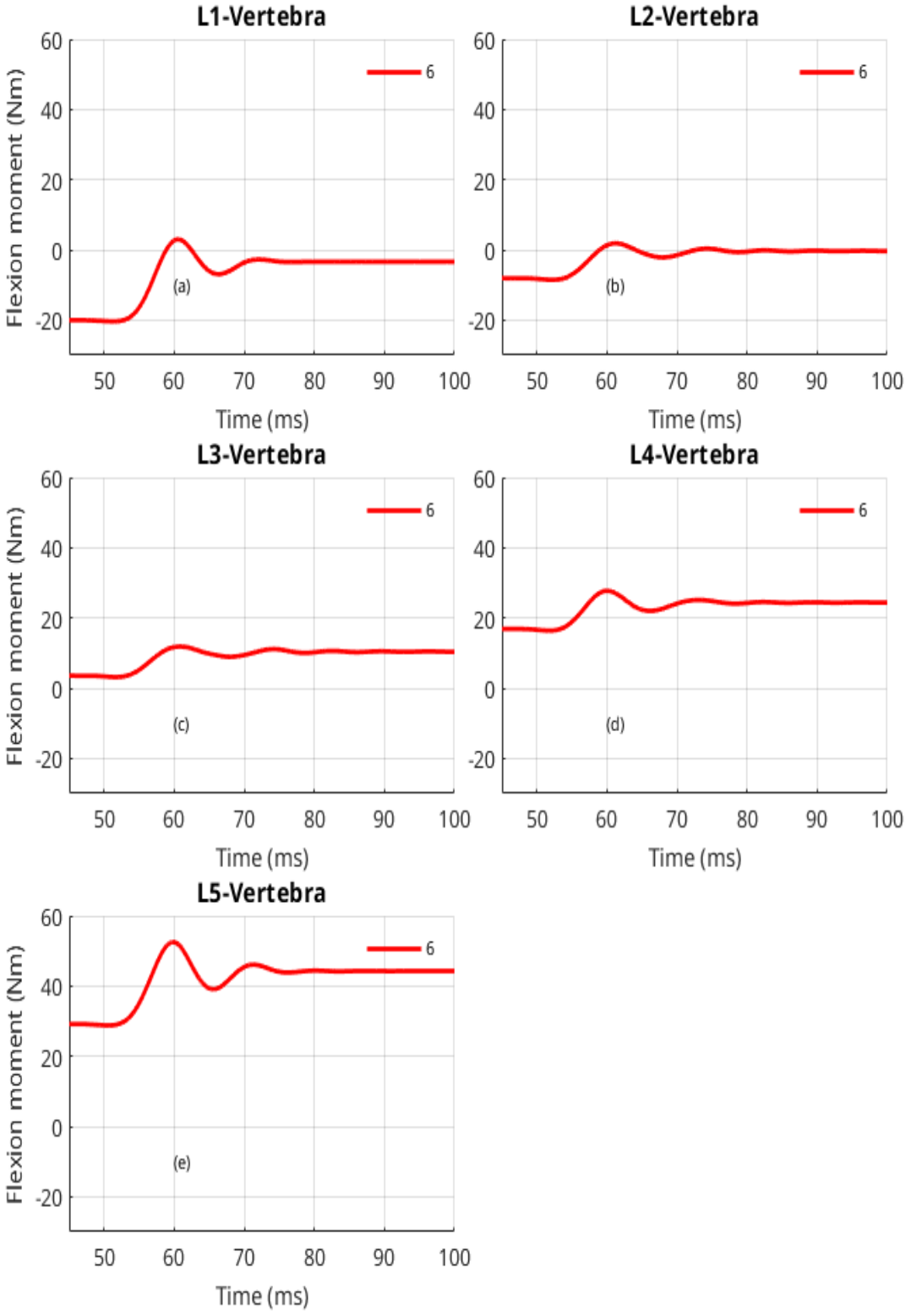

Figure 36. The bending cross section moment versus time in L1 (a), L2 (b), L3 (c), L4 (d) and L5 (e)-vertebra, during the applied loading.

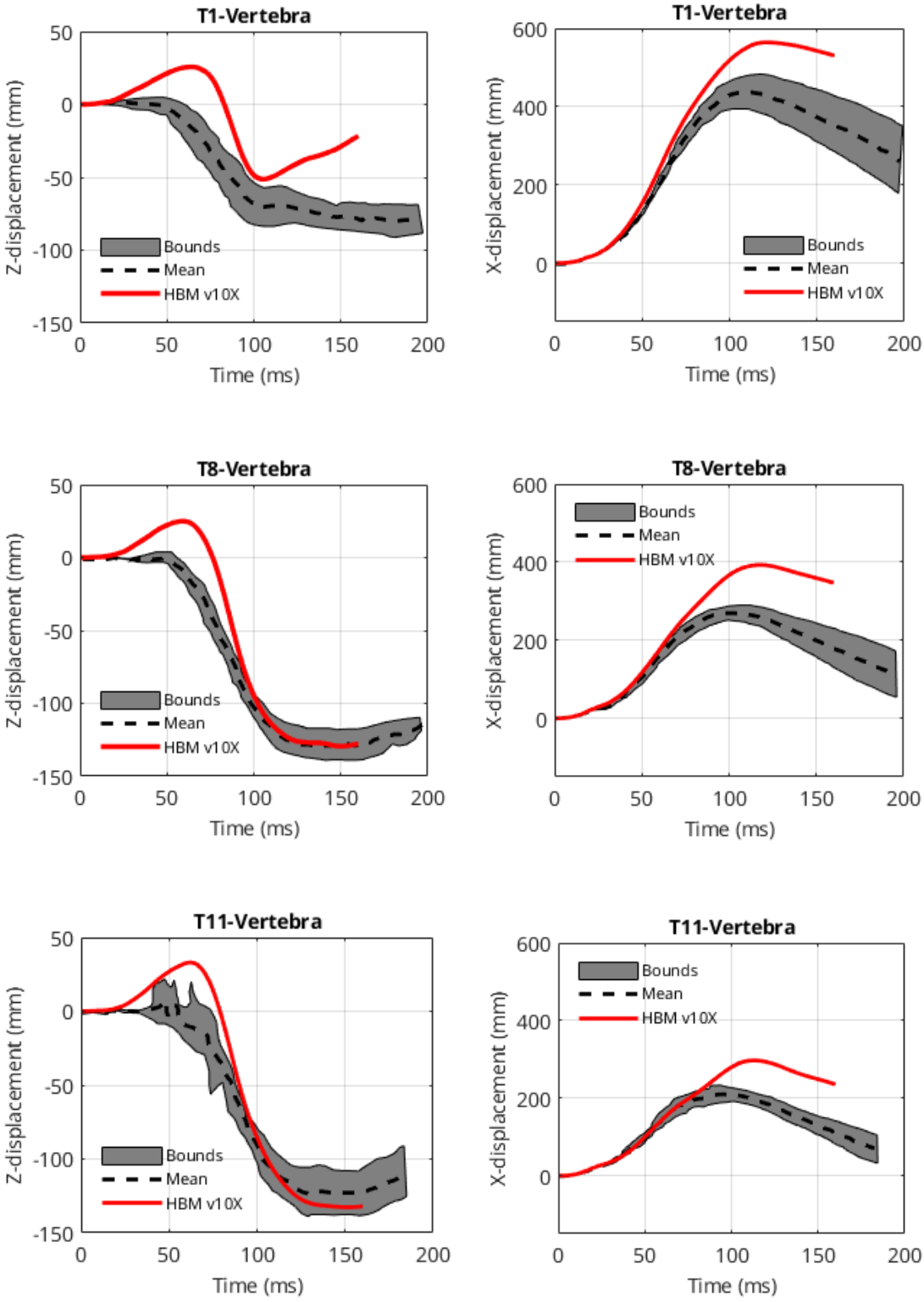

Figure 37. T1, T8 and T11 X and Z displacement time histories. PMHS bounds vs HBM v10X.

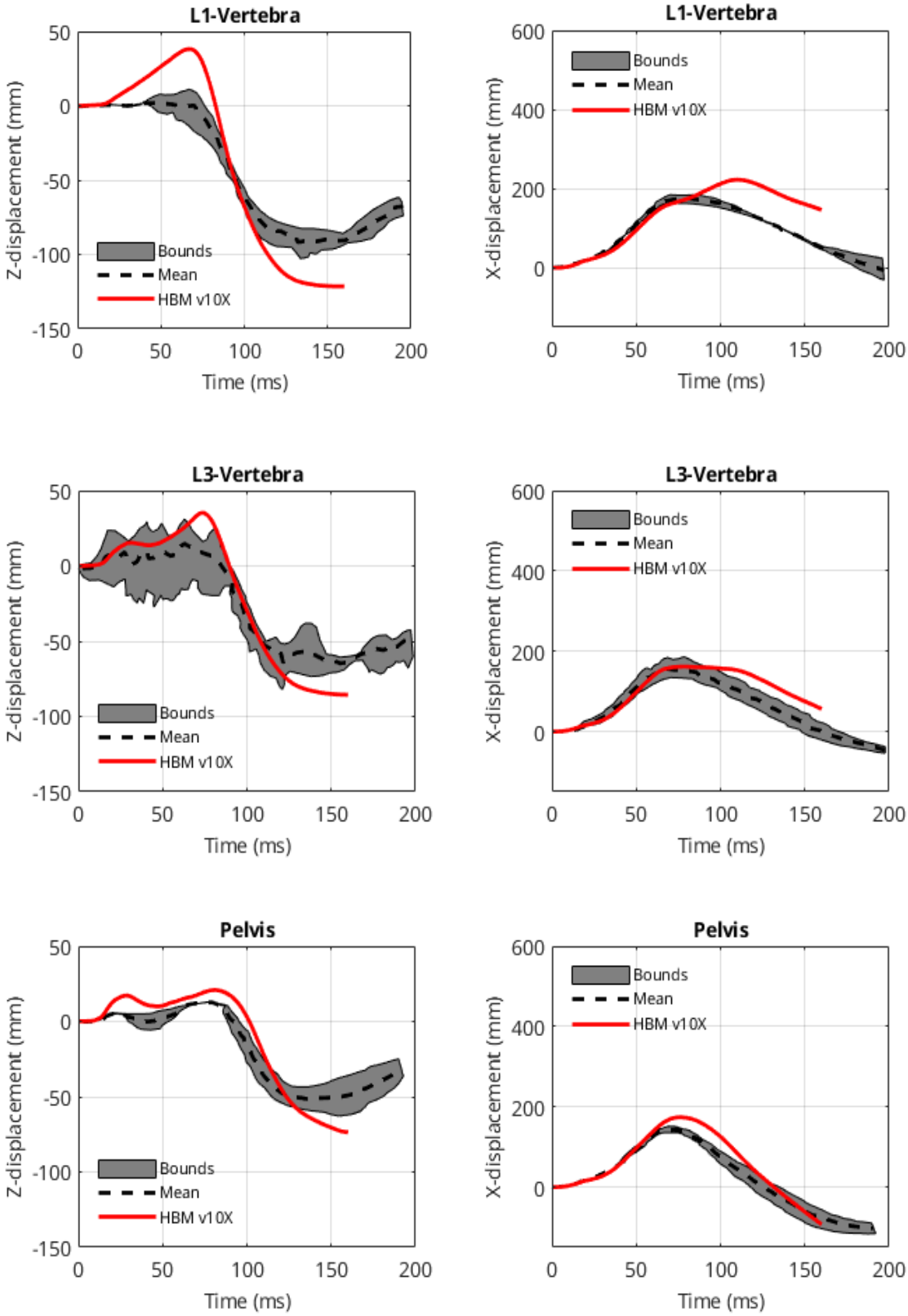

Figure 38. L1, L3 and Pelvis X and Z displacement time histories. PMHS bounds vs HBM v10X.

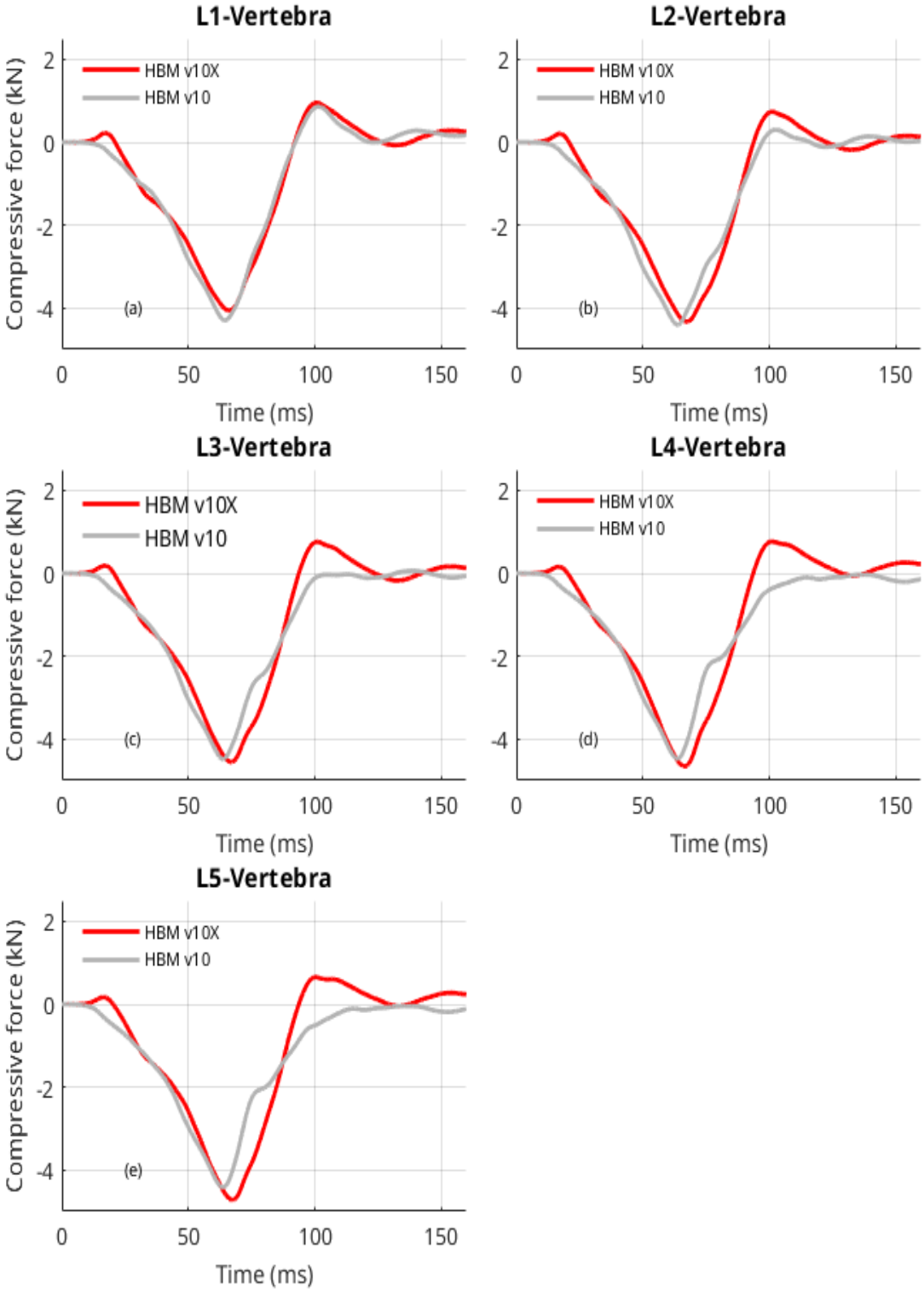

Figure 39. Time histories of the SAFER HBM v10 and v10X compressive cross section force in L1 (a), L2 (b), L3 (c), L4 (d) and L5 (e) vertebra obtained from the HBM in laboratory setting.

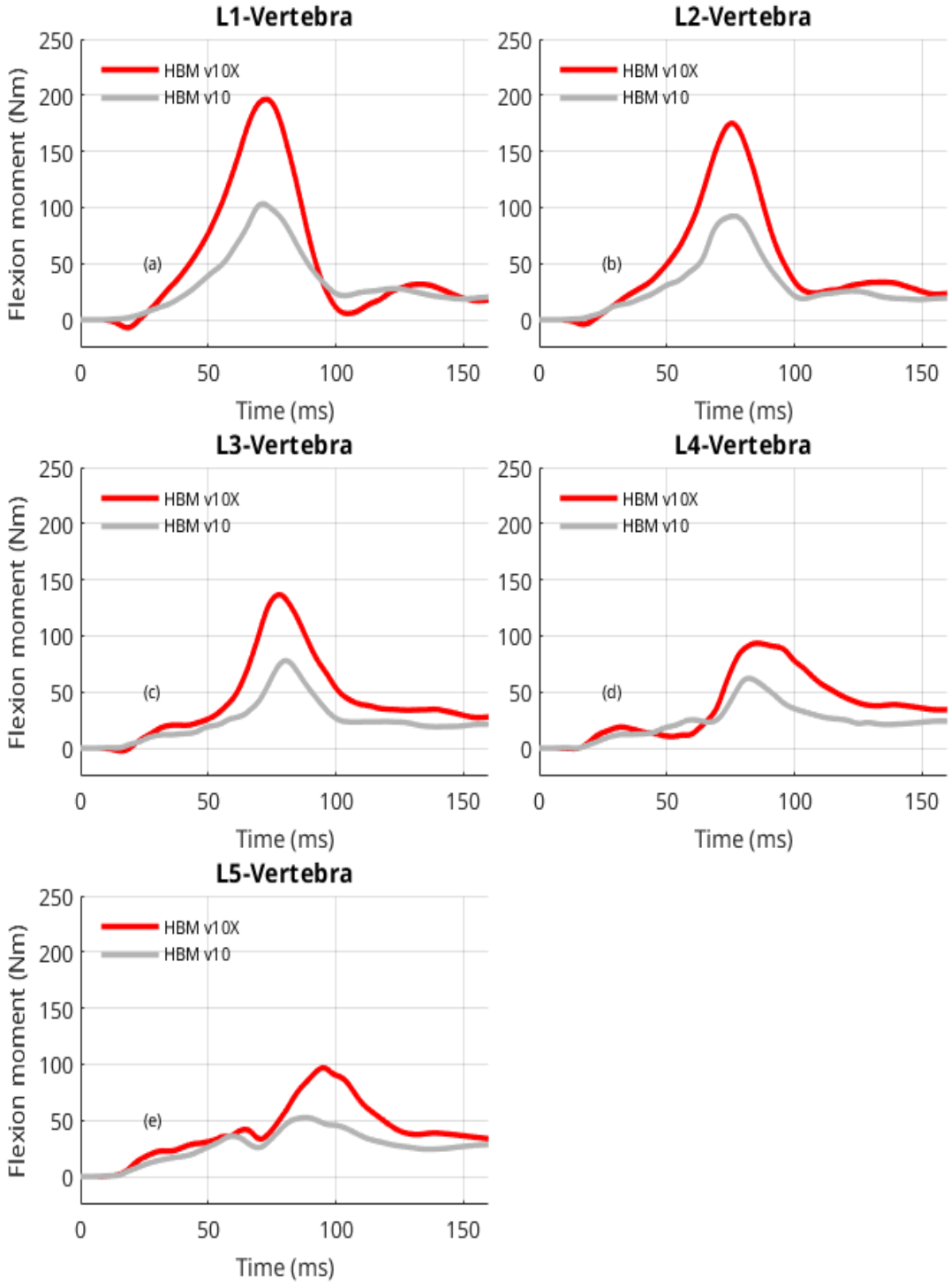

Figure 40. Time histories of the SAFER HBM v10 and v10X bending cross section moment in L1 (a), L2 (b), L3 (c), L4 (d) and L5 (e) vertebra obtained from the HBM in laboratory setting.

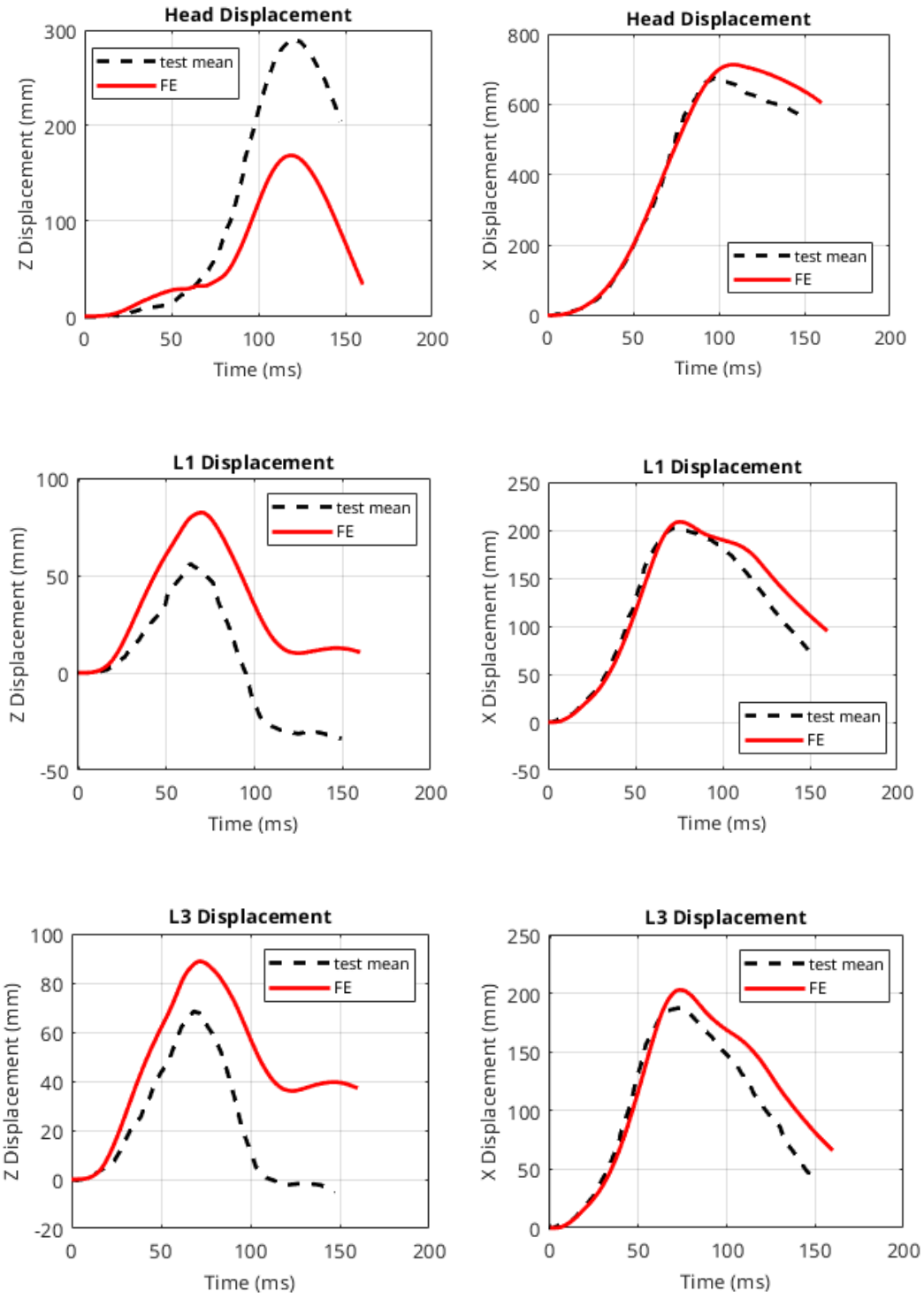

Figure 41. Head, L1, L3 X and Z displacement time histories. THOR FE model vs average of test data.

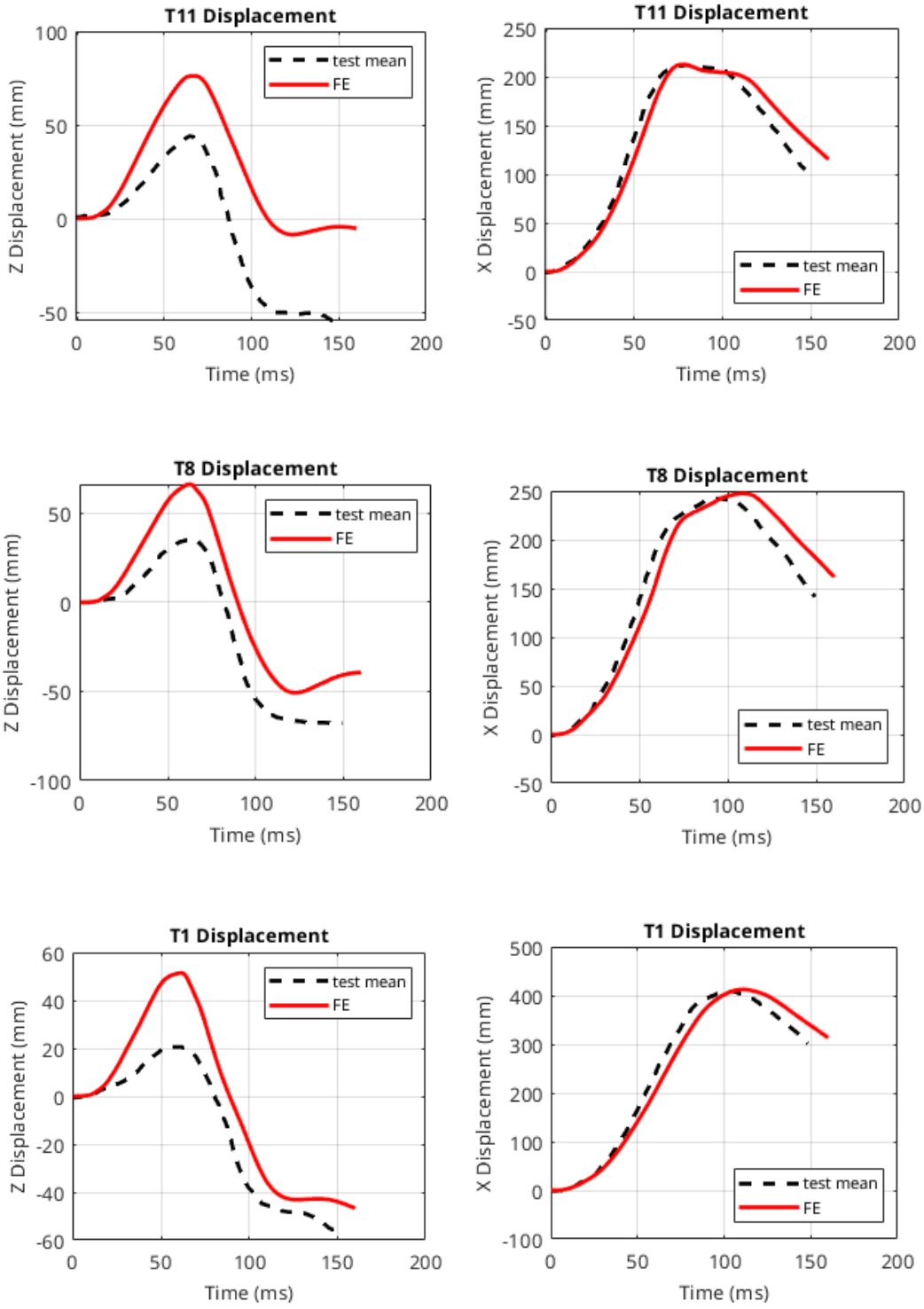

Figure 42. T11, T8, T1 X and Z displacement time histories. THOR FE model vs average of test data.

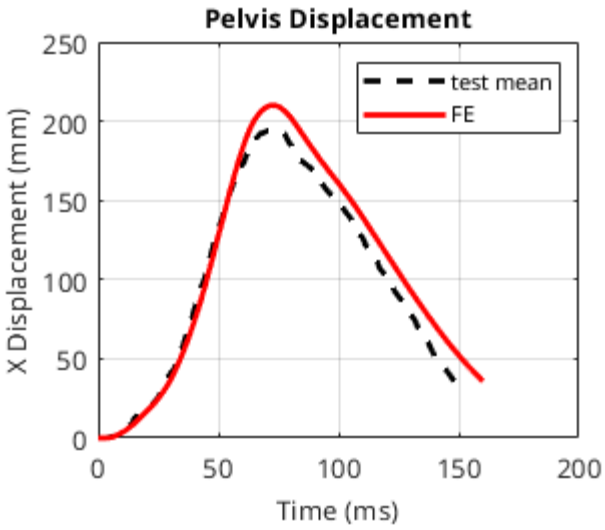

Figure 43. Pelvis X and Z displacement time histories. THOR FE model vs average of test data.

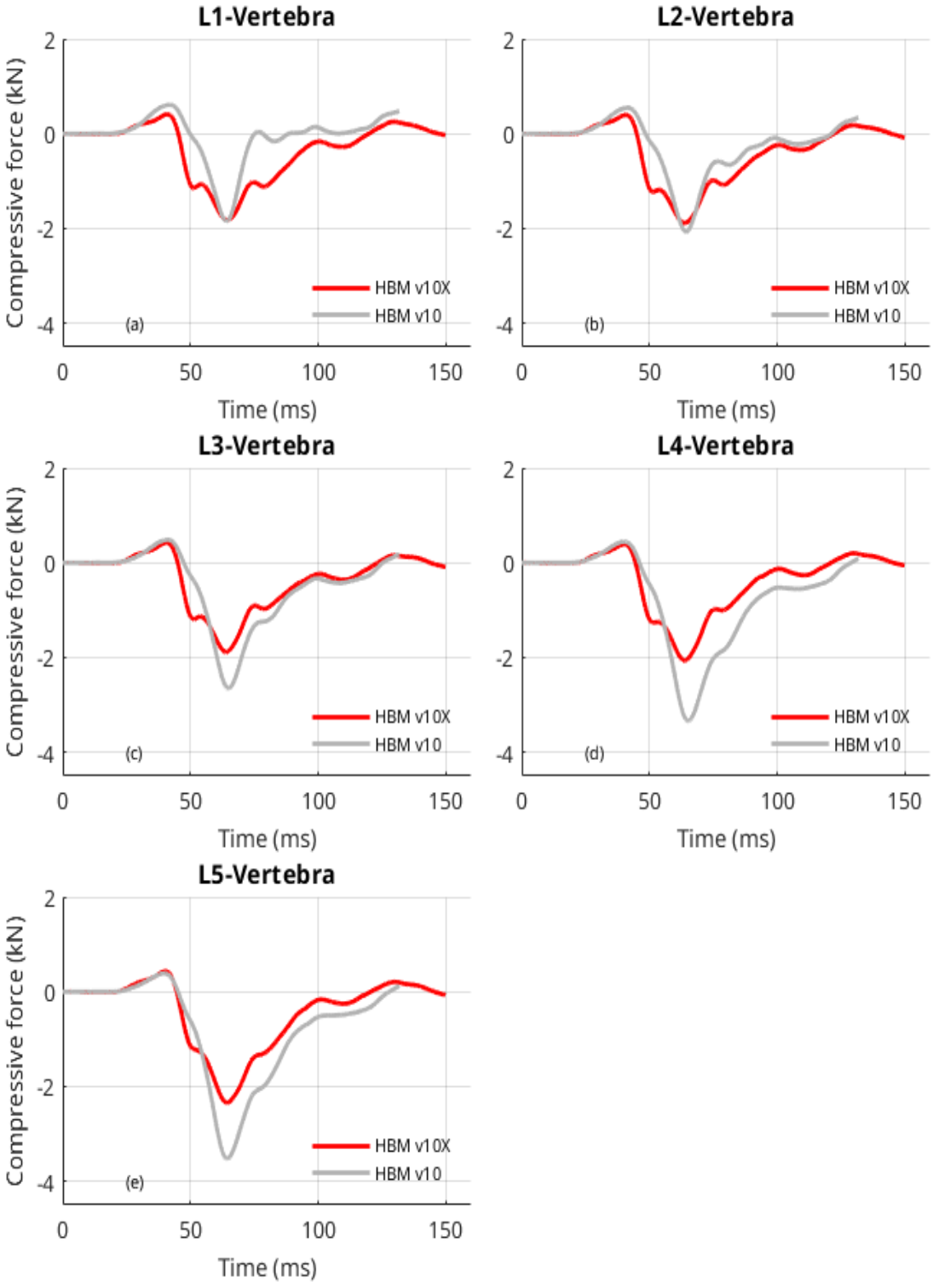

Figure 44. Time histories of the SAFER HBM v10 and v10X compressive cross section force in L1 (a), L2 (b), L3 (c), L4 (d) and L5 (c) vertebra obtained from the accident reconstruction.

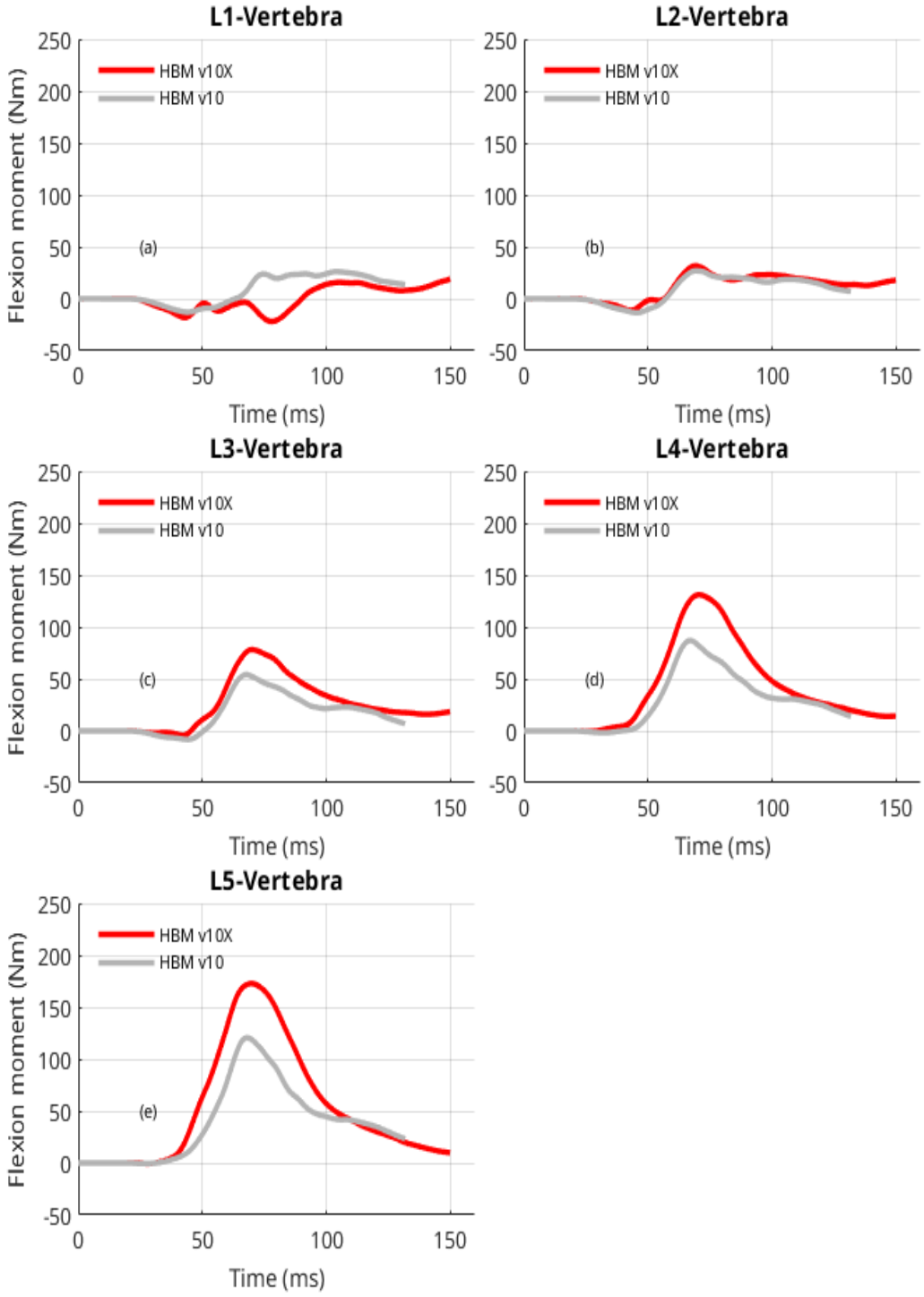

Figure 45. Time histories of the SAFER HBM v10 and v10X bending cross section moment in L1 (a), L2 (b), L3 (c), L4 (d) and L5 (c) vertebra obtained from the accident reconstruction.

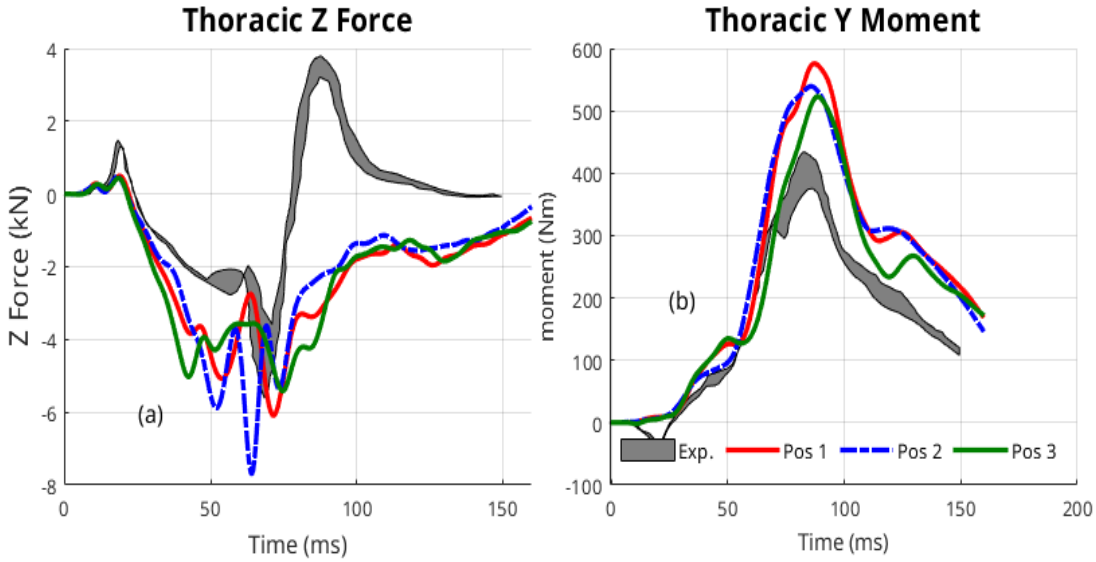

Figure 46. Thoracic compressive force and flexion moment obtained from THOR sled simulation for three different H-point positions on the sled and compared with the test results of Shin et al. (2022).

DEPARTMENT OF MECHANICS AND
MARITIME SCIENCE
CHALMERS UNIVERSITY OF TECHNOLOGY
Gothenburg, Sweden 2023

CHALMERS
UNIVERSITY OF TECHNOLOGY